Inter-comparison of black carbon measurement methods for simulated open biomass burning emissions

Hanyang Li[1], Kara D. Lamb[2, 3], Joshua P. Schwarz[2], Vanessa Selimovic[4], Robert J. Yokelson[4], Gavin R. McMeeking[5], and Andrew A. May[1]

[1] Department of Civil, Environmental, and Geodetic Engineering, College of Engineering, The Ohio State University, Columbus, OH, USA

[2] Earth Systems Research Lab Chemical Sciences Division, National Oceanic and Atmospheric Administration, Boulder, CO, USA

[3] Cooperative Institute for Research in the Environmental Sciences (CIRES), University of Colorado, Boulder, Boulder, CO, USA

[4] Department of Chemistry, University of Montana, Missoula, MT, USA

[5] Handix Scientific, Boulder, CO, USA

Corresponding author: Andrew A. May (may.561@osu.edu).

Abstract

Biomass burning (BB) is a major source of black carbon (BC), but comparing BC content of different smoke-impacted air masses may be uncertain if different measurement techniques are used to quantify the BC, or if non-BC fractions influence a given measurement. To investigate these potential issues, five instruments reporting BC were compared in well-mixed smoke during the FIREX laboratory campaign in 2016, including two filter-based absorption instruments; one *in situ* absorption instrument; a laser-induced incandescence instrument; and a thermal-optical instrument. BB aerosols were generated using fuels common to wildfires in the Western US in a relatively controlled environment, with BC concentrations ranging from roughly 10 to 100 μg m^{-3} (55 total fires). Applying the Bland-Altman graphical approach, systematic biases and proportional biases were identified between the selected reference instrument (*in situ* absorption) and the other four instruments. BC emission factors (EF_{BC}) derived from the thermal-optical instrument, laser-induced incandescence instrument, and filter-based absorption instruments were, on average, 83%, 39% and 66%, greater than the *in situ* absorption instrument, respectively. To understand why these differences exist, principal component analysis combined with a K-means clustering algorithm was implemented to group different fires into three clusters based on several co-dependent fire-related parameters (modified combustion efficiency (MCE),

single scattering albedo (SSA) at 870nm, organic carbon / elemental carbon ratio (OC/EC ratio), and absorption Ångström exponents (AAE)); clusters are nominally referred to as "Black", "Mixed", and "Brown" based on the mean SSA and AAE values for each. The best agreement among all instruments was observed for the "Black" cluster (mean EF_{BC} ratio = 1.89, for the fires with mean SSA = 0.31 and AAE = 1.44); this agreement worsened for the "Mixed" (mean EF_{BC} ratio = 2.94, for the fires with mean SSA = 0.80 and AAE = 1.92) and "Brown" clusters (mean EF_{BC} ratio = 3.12, for the fires with mean SSA = 0.96 and AAE = 2.50), likely due to the increased presence of externally (or internally) mixed aerosols that altered the chemical and optical properties of the aerosols. In general, the discrepancies observed among the BC instruments from this work agree with or slightly exceed the ones from previous ambient and laboratory studies. Care should be taken when interpreting different BC measurements in BB smoke because large artifacts can occur due to co-emitted materials.

1. Introduction

Black carbon (BC, light-absorbing carbonaceous aerosol that absorbs all wavelengths of solar radiation and is chemically inert, Kirchstetter et al. (2004) and Petzold et al. (2013)) aerosol remains an uncertain but important climate forcer, with a recent estimate putting its direct radiative forcing near 0.6 W m^{-2} (Wang et al., 2016). Uncertainty in BC forcing arises in part from the different methods used to measure its concentration in the atmosphere, and comparing measurements with model-predicted values and related radiative forcings (Bond et al., 2013). Methods for measuring BC fall into three broad measurement techniques : optical methods, which measure light absorption or attenuation and convert to an equivalent BC mass (eBC) via assumed mass absorption cross sections (MAC) (Petzold et al., 2013); thermal-optical analysis (TOA) methods, which measure carbon present in filter samples and broadly categorize it into elemental (EC) and organic (OC) carbon fractions; and laser-induced incandescence (LII) methods, which relate thermal emissions to the mass of refractory material present in sampled particles (rBC) (Lack et al., 2014). The response of the instruments to BC can vary due to natural differences in the chemical and optical properties of the sampled BC-containing particles. For example, absorption properties depend on mixing state, shape and size (Bond et al., 2006; Fuller et al., 1999; Jacobson, 2000); LII response has been shown to have some variability in response to different rBC materials (Schwarz et al., 2006); and EC measurements can be affected by co-sampled species (Khan et al., 2012). Sampling artifacts also affect comparisons between instruments; these artifacts can arise from particle-filter interactions, relative humidity (RH) effects, and a myriad of other processes (e.g., Bond et al. (1999); Lack et al. (2008); Liousse et al. (1993); Müller et al. (2011); Murphy et al. (2009); Weingartner et al. (2003)).

Previous studies have compared the different BC measurement methods, usually to either laboratory-generated BC, or to ambient air in a variety of environments (e.g., Müller et al. (2011); Sharma et al. (2017); Sheridan et al. (2005); Watson et al. (2005) and references within; Yelverton et al. (2014)). In general, instruments using the same technique (i.e., for eBC, rBC, or EC) have agreed to within 10-15% in previous inter-comparison studies (Cross et al., 2010; Laborde et al., 2012b; Müller et al., 2011; Slowik et al., 2007). For example, Sheridan et al. (2005) focused on comparing filter-based and *in situ* absorption measurements and reported good agreement provided adequate correction schemes were implemented. However, results from comparisons between different techniques (e.g., rBC against eBC) using various sources of BC showed a much wider range of responses.

Recent laboratory-based inter-comparisons examining different measurement techniques have generally used flame-generated and/or surrogate materials such as fullerene soot or regal black, with some also examining effects of mixing or coating with non-absorbing material. For example, Yelverton et al. (2014) measured emissions from an ethylene-air diffusion flame and found eBC (using both filter-based and *in situ* measurements) to be at least 50% higher than measurements of rBC and EC, from a Single Particle Soot Photometer (SP2) and several different TOA analysis protocols, respectively. Greater values for optical measurements can be explained in part by the enhancement of absorption from internal mixing of BC with non-BC materials (Fuller et al., 1999), though these effects are not always straight-forward (e.g., Cappa et al. (2012); Fierce et al. (2016)). The use of a heated inlet can reduce this effect by volatilizing at least some of the coatings, with good agreement reported between LII, TOA and a filter-based optical method reported for ambient air in Japan (Kondo et al., 2011).

Other groups have examined the response between different instruments for ambient air (e.g., Ajtai et al. (2011); Jeong et al. (2004)). Hitzenberger et al. (2006) reported good agreement between filter-based eBC and EC measurements in a diesel-dominated urban area. More recent work has reported differences between methods for measurements in industrial regions (Miyakawa et al., 2016) and for on- and near-road measurements made with a suite of instruments sampling on a mobile platform deployed on-road (Holder et al., 2014). Sharma et al. (2017) reported that both eBC and EC were roughly three times greater than rBC measured at a remote Arctic site.

Few studies, however, have examined the responses of instruments to biomass burning (BB) emissions specifically, despite its importance as a global BC source; in fact, open BB is estimated to account for approximately 42% of global BC emissions (Bond et al., 2013). Reid et al. (1998) found that different eBC measurements in BB plumes over Brazil agreed within 5%, but EC measurements were about 50% lower. Both Cheng et al. (2011) and Reisinger et al. (2008) noted that ambient BB impacts increased the discrepancy between EC values measured using different temperature protocols. Moreover, McMeeking et al. (2009) showed increasing disagreement between TOA protocols for BB samples with higher OC/EC ratios. Even fewer have examined different instrument responses to BB emissions in relatively controlled environments, and those that have generally focus on cookstove emissions or other types of contained combustion (de la Sota et al., 2017).

To address the relative lack of inter-comparison measurements for BC from BB, we conducted a systematic comparison of different BC instruments spanning all measurement techniques under relatively controlled laboratory conditions. Our study focuses on a detailed comparison of five BC measurement instruments during the Fire Influence on Regional to Global Environments Experiment (FIREX) laboratory campaign in 2016. The purpose of our study was to quantify any differences in measurements of eBC, rBC and EC derived from commonly-used BC instrumentation for different biomass fuels under different combustion conditions.

2. Methodology

2.1. Sampling site and experimental methods

The FIREX campaign was conducted at the United States Forest Service Fire Science Laboratory (FSL) from October 1 to November 15, 2016 in Missoula, Montana. More than 100 burns were

performed in an "open" combustion environment under artificial control of fuel types and quantities. A summary of the fuels, fuel components, and fuel properties (e.g., moisture content) is provided as Table S1. A more detailed description of the combustion facility and burn information can be found in Koss et al. (2018) and Selimovic et al. (2018).

We used an 8" diameter semi-rigid aluminum main transfer duct to transfer the smoke from the combustion room to the FSL's wind tunnel room, where our BC instruments were located. The flow rate through the duct was roughly 20,000 LPM, resulting in a residence time of 1 to 1.5 s; at this residence time, we expect minimal losses within the transfer duct. We drew the emissions into our sampling chamber (~200 LPM, anisokinetic sampling) from the center of the duct to minimize wall interactions using a 2.5 cm stainless steel tube. We did not quantify leaks or losses through this transfer line since our work focuses on an inter-comparison of the different BC instruments rather than the accurate quantification of BC mass emissions from the fires; any leaks/losses would affect all instruments.

We used a design similar to that used by Sheridan et al. (2005) to transfer the emissions to the BC instruments. Emissions first passed through a cyclone (Model URG-2000-30ET, URG Corp., estimated to have a 1.5-µm cut-point at a flow rate of 200 LPM) to remove larger particles. The emissions that passed through the cyclone were injected into an actively-mixed cylindrical chamber (stainless steel, volume = 210 L). This chamber served as an intermediate between the transfer line and the BC instrumentation to minimize biases that could arise when sampling at different flow rates and locations from the main transfer duct. Valves allowed us to either pull BB emissions from the transfer line or introduce HEPA-filtered air to the sampling chamber. During experiments, emissions were sampled from the mixing chamber into eight real-time BC instruments and two sets of filters. Filtered air was drawn into the mixing chamber during the experiments to replace the air sampled by the BC instruments and filters, leading to a gradual dilution of particle concentrations in the mixing chamber over time. A schematic of this setup is provided in Figure S1 and Figure S2, and a more detailed description of the experiments is available in the Supplementary Material.

Two types of experiments were performed during FIREX: stack burns, where emissions were sampled in real-time through an exhaust stack over the fire; and room burns, where emissions filled the combustion room (12.5m × 12.5m × 22m) and were then intermittently sampled by instruments over several hours. During stack burns, we sampled emissions from the initial stage of the burn (typically flaming combustion) up until achieving a BC concentration in the sampling chamber between 10 to 100 µg m^{-3}. However, in some instances, we deliberately sampled only during the later stages of the fire to collect samples with a larger contribution from smoldering combustion, and hence, a potentially broader range of aerosol optical properties which might be observed near the source for real-world fires. For room burns, we followed the similar approach outlined for stack burns, but in this case, only well-mixed emissions in the combustion room were sampled (determined by approximately stable real-time absorption values of other study participants' instruments). In this case, the room itself acted to integrate the emissions of the entire fire, a sub-sample of which was then drawn into our chamber. Due to the relatively long residence time in the combustion room (on the order of hours due to limited air exchange), we were able to collect multiple emission samples from the room into our mixing chamber for each room burn.

2.2. Instrumentation

We deployed a suite of instrumentation to characterize BC in the smoke samples during the campaign, including two *in* situ methods for eBC, five filter-based methods for eBC, and one method for rBC. Furthermore, two 47mm filter holders were used for off-line thermal-optical analysis of EC; one contained a single (bare) quartz filter (Q), while the other contained a Teflon filter followed by a quartz filter (QBT). Table 1 lists all of the key BC instrumentation included in our study, as well as their measured parameters and key specifications used for this inter-comparison work. Note that we are using the BC instruments per manufacturer instructions and did not adopt non-standard procedure to enhance their performance specifically for BB smoke in this work. In addition to the BC instruments, we deployed a carbon dioxide (CO_2) gas analyzer (LI-840A, LI-Cor Biosciences), a carbon monoxide (CO) gas analyzer (model T300, API-Teledyne), and scanning mobility particle sizer (model 3938, TSI Inc.).

Table 1 Summary of BC instruments used during the 2016 FIREX laboratory campaign

Method	Instrument (Manufacturer)[a]	Abbr.	Direct Measurement	Derived parameter used in current work[b]	Measurement uncertainty (Relative)	Other notes
Thermal-optical (EC)	OCEC Analyzer (Sunset Laboratory Inc)[c]	Offline OCEC	OC and EC area density on filter (μg m^{-2})	BC mass concentration (μg m^{-3}), OC/EC ratio	16% (Liu et al., 2013)	Analyze using IMPROVE-A TOR temperature protocol.
In situ absorption (eBC)[d]	Photoacoustic Extinctiometer (Droplet Measurement Technologies, Model 870 nm)	PAX-870	B_{abs} and B_{scat} at 870 nm (Mm^{-1})	BC mass concentration (μg m^{-3}), SSA, AAE and SAE (inferred with the PAX-405)	20% (Nakayama et al., 2015)	Use MAC of 4.74 m^2 g^{-1} converted to 870 nm from recommended value in Bond and Bergstrom (2006).
	Photoacoustic Extinctiometer (Droplet Measurement Technologies, Model 405 nm)[e]	PAX-405	B_{abs} and B_{scat} at 405 nm (Mm^{-1})	AAE and SAE (inferred with the PAX-870)	7% (Nakayama et al., 2015)	-
Filter-based absorption (eBC)[d]	Aethalometer (Magee Scientific)	AE-31	B_{atn} at seven wavelengths (370, 470, 520, 590, 660, 880, and 950 nm) (Mm^{-1})	Not included in current work[f]		
	Micro Aethalometer (AethLabs)	μAE	B_{atn} at 880 nm (Mm^{-1})			
	Atmospheric Black Carbon Detector (Lawrence Berkeley National Laboratory)	ABCD	B_{atn} at 880 nm (Mm^{-1})			
	Continuous Light Absorption Photometer (NOAA ESRL GMD)[g]	CLAP	B_{atn} at 467, 528, and 652 nm (Mm^{-1})	BC mass concentration (μg m^{-3}), AAE, B_{abs} at 870 nm (Mm^{-1})	30% (Ogren et al., 2017)	Apply flow and pressure corrections. Apply filter type correction on the samples of CLAP equipped with Azumi filter. Perform correction using B1999 scheme and its empirical parameters. Use PAX-derived Bscat and SAE to compute Bscat at TAP and CLAP wavelengths (needed in the correction

	Tricolor Absorption Photometer (Brechtel Manufacturing Inc)[g]	TAP	B_{atn} at 467, 528, 652 nm	BC mass concentration (μg m^{-3}), AAE, B_{abs} at 870 nm (Mm^{-1})	30% (Laing et al., 2016)	scheme). Convert self-derived Babs to that at 870 nm with self-calculated AAE. Use the same MAC as the PAX-870.
Refractory (rBC)	Single Particle Soot Photometer (Droplet Measurement Technologies)[h]	SP2	Laser induced incandescence and light scattering of single particle	BC mass concentration (μg m^{-3})	20% (Laborde et al., 2012a)	Observed particle mass distribution is fitted by a log-normal size distribution. A non-standard laminar flow element is used to measure flow rates accurately.

[a] More detailed information of the instruments (such as flow rate and spot area of filter-based instruments) is provided in Table S4.
[b] In our comparison, the generic term BC is used to refer to one of the three methods: eBC, EC, and rBC.
[c] The filters were collected for 76 experiments during the campaign, generally 2 or 3 per day.
[d] Operating wavelengths are based on manufacturer specifications. B_{atn} is similar to the B_{abs} but it is specific to filter-based instruments.
[e] The PAX-405 was used from fire 32 to fire 107.
[f] See Section 2.2.3 for details.
[g] B1999 correction scheme was performed on the CLAP and TAP data from fire 32 to fire 107, during which we have both PAX-405 and PAX-870.
[h] The SP2 was only used during the stack burns (fire 1 to fire 75).

2.2.1. Determination of EC from filter samples

We used a TOA method to determine EC on the Q and QBT filters. Prior to the campaign, the quartz filters were baked at 550 °C in air for a minimum of 8 hr to remove possible organic contamination. Both quartz and Teflon filters were kept in pre-baked-aluminum-foil-lined petri dishes sealed with Teflon tape, and stored in a freezer (-18 °C) before and after sampling. Filters were sampled for approximately fifteen minutes to ensure sufficient sample loading for detection. After collection, the valve connecting the filters to the chamber was closed, and the filters were removed and returned to their respective petri dish. To check for contamination, some filters served as handling blanks (filters brought to the campaign but not loaded in the filter holders), and roughly 10% of all filters were dynamic blanks (filters loaded in the filter holders that sampled filtered air through the barrel).

Filters were analyzed in the laboratory at The Ohio State University's campus using a Sunset OCEC Analyzer (hereafter referred to as offline OCEC) following the study. We used both the US Interagency Monitoring of Protected Visual Environments (IMPROVE-A) thermal optical reflectance (TOR) protocol (Chow et al., 1993) and the National Institute of Occupational Safety and Health protocol (Birch and Cary, 1996) with maximum temperature 870 °C (NIOSH-870), and a comparison between the two protocols can be found in Figure S4. However, we will primarily focus on the discussion of IMPROVE-A TOR results in the main text because this method is more commonly used in the analysis of ambient samples (Solomon et al., 2014). Briefly, these methods provide OC and EC concentrations from the Q and QBT filters. Measurements of laser reflectance throughout the analysis assist in the split of OC and EC due to the pyrolysis carbon (PC) generated during the analysis of OC stages. The production of and correction for PC is subject to the thermal and optical protocols and can lead to uncertainties in the split carbon concentration (Chow et al., 2004). The instrument was calibrated daily using clean filters and sucrose standards.

Analysis of handling blanks yielded averaged total carbon (OC + EC) and EC concentrations of 0.72 ± 0.27 μg m^{-2} and 0.03 ± 0.05 μg m^{-2}, respectively (detection limit was 0.08 μg m^{-2} for both), suggesting almost no contamination throughout the shipping and handling of samples, especially for EC. The analysis of dynamic blanks also suggests almost no contribution to EC (0.09 ± 0.07 μg m^{-2}) from any residual contamination in our experimental setup.

2.2.2. *In situ* eBC measurements

The *in situ* aerosol optical properties were measured by two photoacoustic extinctiometers (PAX) at 870 nm and 405 nm from Droplet Measurement Technologies (DMT), which will be subsequently referred to as the PAX-870 and PAX-405, respectively. Briefly, the PAX measures light absorption coefficients (B_{abs}) and scattering coefficients (B_{scat}) (Arnott et al., 1999; Nakayama et al., 2015). Emission samples entering both instruments were first passed through a scrubber to remove nitrogen dioxide and other UV-absorbing gases (which may interfere with the PAX-405 measurements) and a diffusion drier to minimize the effects of RH on the measured optical properties, following the manufacturer recommendations. The scrubber and drier were recharged as needed throughout the campaign. We only include eBC from the PAX-870 in this inter-comparison because the contributions of brown carbon (BrC) to absorption at 405 nm can be significant (Andreae and Gelencsér, 2006). The manufacturer-recommended MAC value of

4.74 m^2 g^{-1} at 870 nm is used to convert B_{abs} to eBC mass in current work for both the *in situ* and filter-based methods.

2.2.3. Filter-based methods for eBC

Five filter-based instruments provided real-time light absorption measurements; however, a direct comparison between the Magee Scientific AE31 and the filters for offline OCEC analysis was not possible due to frequent AE31 filter-tape advancement at higher concentrations, so the AE31 is not included in this work. However, the AE31 along with the prototype Atmospheric Black Carbon Detector (ABCD) and Micro Aethalometer (μAE), will be considered in future work. Consequently, the only filter-based eBC results that we include here are from the Tricolor Absorption Photometer (TAP) from Brechtel Manufacturing Inc (BMI) and Continuous Light Absorption Photometer (CLAP) from NOAA's Earth System Laboratory's Global Monitoring Division, which are widely used in monitoring networks.

Both CLAP and TAP are photometers that provide light absorption measurements of particles deposited on a filter, similar to the Particle Soot/Absorption Photometer (PSAP) (Ogren et al., 2017), but with multiple filter spots (8 sample spots and 2 reference spots), thus enabling longer operation between filter changes. These instruments are conceptually similar to each other (and the PSAP), providing light absorption measurements at three wavelengths (467 nm, 528 nm, and 652 nm); however, BMI substantially re-engineered the CLAP in their development of the TAP. The spot change of the CLAP was manually performed when transmission (Tr) reached approximately 0.5, while the TAP advanced to a new spot automatically with a Tr threshold set to be 0.5. For the first portion of the campaign, we used Pallflex E70-2075S filters in the CLAP while Azumi filters (model 371M, Azumi Filter Paper Co., Japan) were used in the second portion (due to a lack of availability of the Pallflex filters). The TAP was equipped exclusively with the Azumi filters throughout the campaign. We applied the correction recommended in Ogren et al. (2017) to account for these differences in filter material when converting to Azumi filters.

One challenge with any filter-based instrument is that the presence of the filter can potentially introduce biases. For example, high filter loadings may result in an under-estimate of light absorption due to the reduction of filter optical path by deposited particles, while light scattering by embedded particles or the filters themselves can result in an over-estimate due to their contribution to the decrease of transmittance. Various correction schemes exist to account for these biases (e.g., Bond et al. (1999), Ogren (2010), Virkkula et al. (2005), and Virkkula (2010)). However, to simplify our inter-comparison efforts here and reduce uncertainties that may be introduced by different schemes, we will solely use the widely adopted correction factor from Bond et al. (1999) in this work, hereafter referred to as "B1999" for both the TAP and CLAP data. This scheme was built into the TAP software and was routinely used in NOAA's processing of CLAP data. A comprehensive comparison of all of the filter-based instruments, as well as the evaluation of multiple published correction equations for these instruments, will be the focus of future work.

2.2.4. Incandescence technique for rBC

We measured rBC concentrations with a DMT SP2 (only available to us during stack burns). Briefly, the SP2 uses LII to quantify the mass of rBC in particles, here in the range of

approximately 1 and 160 fg (a mass equivalent diameter range of 90-550 nm, assuming that rBC has a void free density of 1.8 g cm^{-3}). The instrument also detects the single particle light scattering and provides information that can be used to calculate BC-containing particle optical size and mixing state. In the current study, data was recorded discontinuously during the experiments with high particle concentrations, and an exponential decay curve was fit to the data to interpolate rBC mass concentrations between measurement periods (an example of time-series BC results from the four near-real-time instruments throughout a fire is shown in Figure S3). A lognormal fit on the particle mass distribution (Schwarz et al., 2006; Spackman et al., 2008) was used to derive correction factors (Table S2) to account for any BC outside the instrument detection limits during each experiment. These factors, which ranged from 1.00 to 1.18, were used to correct the SP2-observed rBC mass concentrations to a best-estimate of the total accumulation mode rBC concentration. During FIREX, the SP2 was equipped with a non-standard laminar flow element designed to measure lower flow rates accurately, with the SP2 sampling at flow rates on the order of 0.006 LPM to minimize coincidence errors and other complications associated with high particle count rates. This low sample flow was carefully calibrated, and only added a small component of additional uncertainty (~<5%) to the SP2 concentration measurement. Coincident incandescent particles (e.g. two particles measured in a single SP2 detection window of ~80 μs) were not taken into account during processing; these could lead to an under-estimation of rBC mass during sampling periods with high aerosol concentrations. We estimated the worst case (i.e. at the highest concentrations of rBC) resulting low bias in concentration to be at most 5-8% during FIREX.

The leading edge only (LEO) fitting method (Gao et al., 2007) was used to estimate a coating thickness from the initial optical size of individual rBC particles, assuming Mie core-shell theory. A value of n_{core}=2.26+1.26*i* was assumed for the complex index of refraction of the rBC core (Moteki et al., 2010) and $n_{coating}$=1.45 for the non-absorbing coating material at 1064 nm (the wavelength of the SP2 laser) following Lack and Cappa (2010). These values were used in the calculation of absorption enhancement (E_{abs}) discussed in Section 3.2.1.

2.2.5. Calibrations

As part of our sampling strategy, we conducted calibration experiments at various frequencies during the campaign. SP2 laser intensity was calibrated twice-daily with polystyrene latex spheres, following Schwarz et al. (2010). No significant changes in laser efficiency relative to instrument temperature (as has been previously observed in some cases) were observed. Throughout the campaign sufficient laser intensity for detection over the rBC mass range reported (1- 160 fg) was maintained, as per Schwarz et al. (2010). The SP2 rBC mass calibration was performed using fullerene soot (Sigma Aldrich lot #F12SO11) size selected through a differential mobility analyzer (for mobility diameters between 125-350 nm) twice during the campaign, and the two calibrations were within ~10% of one another. The empirical relationship relating the mobility diameter to single particle fullerene soot mass from Moteki and Kondo (2010) was used to determine the mass to incandescence relationship. The average mass to incandescence relationship from these two calibrations was used to process data from the stack burns.

Light absorption and light scattering of the PAXs were calibrated once a week following the manufacturer's recommend procedure using ammonium sulfate aerosol and fullerene soot, respectively. Flow rates of all instruments were measured regularly using a bubble flow meter

and adjusted if necessary. Periodic gas calibrations of the CO_2 and CO analyzers were also performed using standard gas mixtures (2000 ppmv CO_2 in N_2 and 100 ppmv CO in N_2, respectively).

2.3. Calculation of EF_{BC} and key fire-related parameters

To standardize the data across different instruments (with different time resolutions) and across different fires, we calculated a time-integrated EF_{BC} for each fire (where the integration window is fifteen minutes, the offline OCEC filter sampling period):

$$EF_{BC} = \frac{\Delta BC}{\Delta CO_2 + \Delta CO} \times f_C \quad (1)$$

where ΔBC represents the time-integrated, background-corrected BC mass concentration (μg m^{-3}) integrated over the duration of filter collection, and ΔCO_2 and ΔCO are the time-integrated, background-corrected concentrations of CO_2 and CO over the same time interval (converted to g-C m^{-3} from ppmv). We calculated the eBC mass concentration at 870 nm (the operating wavelength of the PAX-870) from B_{abs} by dividing by the MAC. For the CLAP and TAP, we first extrapolated the measured B_{abs} to 870 nm using inferred absorption Ångström exponents (AAE; see below) as others have done previously (Sheridan et al., 2005; Slowik et al., 2007), and then derived eBC mass concentration. This results in different ΔeBC values than at 652 nm for the TAP and CLAP (Figure S5), but we took this approach to compare all of the eBC instruments at the same wavelength (870 nm). The term f_C is the fuel's mass fraction of carbon calculated on a dry weight basis of fuel, which ranged from 0.37 to 0.56 (Selimovic et al., 2018). Because these time-integrated EF_{BC} were sub-sampled from each fire and did not account for any leaks/losses, we do not recommend that these values be used for direct comparison with fire-integrated EF_{BC} from other studies.

We evaluated the combustion conditions that produced the emissions sampled in our chamber using the modified combustion efficiency (MCE), determined by excess CO and CO_2 mixing ratios (also time-integrated over the 15-minute filter sampling period):

$$MCE = \frac{\Delta CO_2}{\Delta CO_2 + \Delta CO} \quad (2)$$

MCE can be used as an indicator of flaming (MCE → 1) or smoldering (MCE < ~0.9) combustion (Akagi et al., 2011; McMeeking et al., 2009; Reid et al., 2005). In this campaign, typical values of ΔCO_2 and ΔCO measured from our chamber ranged from 80-150 ppmv and 2-10 ppmv, respectively. Occasionally, low ΔCO_2 concentrations relative to background led to higher uncertainties in background corrections. Nevertheless, our calculated MCE values generally agreed within 10% of those measured in the combustion room (Selimovic et al., 2018), despite differences in collection times for some fires (Figure S6).

Two other key parameters utilized in our data analysis were the single scattering albedo (SSA; an optical property of emitted aerosol) and the OC/EC ratio (a chemical property of the emitted aerosol). Since the focus of this work is BC, which is the dominant absorber at longer wavelengths, we used measurements of B_{abs} and B_{scat} from the PAX-870 to calculate SSA at 870 nm:

$$SSA = \frac{B_{scat}}{B_{abs}+B_{scat}} \quad (3)$$

The OC/EC ratio was simply calculated as the ratio of the OC mass concentration divided by the EC mass concentration, as derived in the offline OCEC IMPROVE-A analysis.

Another optical property of the emissions that we considered in data interpretation was the AAE, which describes (fits) light absorption as a power law function of wavelength.

$$AAE = -\frac{ln\,(B_{abs}(\lambda_1)/B_{abs}(\lambda_2))}{ln(\,\lambda_1/\lambda_2)} \quad (4)$$

It has been widely accepted that "pure" externally mixed BC has AAE ≈ 1 (Bond et al., 2013; Lack and Langridge, 2013) , while BB aerosols typically have AAE > 1 (Clarke et al., 2007). For example, during previous laboratory studies and in ambient measurements, the AAE was observed to range from 1.5-7 and highly related to SSA (Liu et al., 2014; McMeeking et al., 2014). AAE can be inferred from an instrument (or combination of similar instruments) that measure light absorption at different wavelengths of light. Hence, we could derive AAE from the outputs of both the CLAP and the TAP (exponential least squares fit between multiple B_{abs} and wavelengths; $b_{abs} \sim \lambda^{-AAE}$), or the combination of the PAX-870 and PAX-405 (applying Eq. 4 directly). We observed some discrepancies among the AAEs obtained from these instruments, which may be due to measurement uncertainties of B_{abs} that propagates to the calculation of AAE. Furthermore, the lack of a well-accepted correction algorithm of filter-based instruments will introduce uncertainties on the AAEs derived from the CLAP and TAP (Backman et al., 2014). In our subsequent discussion, we used the average AAE value from all three instruments (referred to as AAE_{avg}). The analogous term for light scattering is the scattering Ångström exponent (SAE), which was needed for the correction of CLAP and TAP data.

2.4. Statistical methods for data processing and analysis

To aid in data interpretation, we used principal component analysis (PCA) combined with K-means clustering (hereafter, shortened to PCA/K-means) to categorize each burn into groups with similar fire-related parameters (Section 3.1.2). We first applied PCA to transform MCE, SSA, and OC/EC ratio into a set of new orthogonal variables (i.e., principal components (PC); Jolliffe (1986)) because each of these parameters has some degree of correlation with the others. After obtaining the PCs, we conducted K-means clustering to obtain K disjoint groups (i.e., groupings of burns, or "clusters") such that the burns in a given cluster have similar PCs and are different from the burns in other clusters (Hartigan and Wong, 1979). The number of clusters was determined based on "elbow criteria", which considers at the total within-cluster sum of squares (total-WCSS, a parameter that describes compactness of the clustering) as a function of the number of clusters (Hardy, 1994). Detailed descriptions of the PCA/K-means procedure performed on FIREX dataset are given in the Supplementary Material.

After categorizing the burns, we adopted the Bland-Altman difference approach (Altman and Bland, 1983) to evaluate the agreement of the five instruments (Section 3.2.1). This approach remains the "gold-standard" for method-comparison studies (Ryan and Woodall, 2005) because it enables visual examination of the agreement and the data scatter between two instruments, where one instrument is arbitrarily chosen as the reference (i.e., it need not be a "ground truth").

It has also been widely used in various aerosol studies to visualize the differences between instruments (Nieuwenhuijsen et al., 2015; Spinazzè et al., 2017; Ward et al., 2006). Briefly, in the Bland-Altman approach, the difference between the two measurements for a given sample is plotted against the two measurements' mean value for that sample. Hence, a good agreement between two methods is observed when the differences are scattered about zero and the best-fit line of the differences has a slope of zero. Conversely, one can also identify systematic biases (i.e., the data are not scattered about zero) and/or proportional biases (i.e., the slope of the data is not zero) between instruments.

Because linear regressions are a more traditional approach in the aerosol science literature than the methods described above, we have also provided these results in the online Supplementary Material. Figure S7 relates EF_{BC} for each instrument with MCE, similar to prior work (Hosseini et al., 2013; May et al., 2014; McMeeking et al., 2009), while Figure S8 relate EF_{BC} between different instruments. However, we have utilized a major axis regression (rather than the more-typical ordinary least squares regression) which accounts for uncertainty in both the abscissae and the ordinates (Ludbrook, 2010; Wu and Yu, 2018).

2.5. Computational methods

Data processing and fire integrations were performed with Igor Pro. Igor Pro's exp_XOffset curve-fit function was used to interpolate data points when CLAP and TAP advanced filter spots during fires and when the SP2 measurements were not recorded. The R programming language was used for statistical analysis (lmodel2 package for type II linear regression, prcomp and kmeans packages for PCA/K-means analysis, and bland.altman.plot package for Bland-Altman figures).

3. Results and discussion

We broadly focus our presentation of results into two sections. Section 3.1 discusses the calculated fire-related parameters (MCE, SSA, OC/EC ratio, and AAE_{avg}) and the outcome of our PCA/K-means clustering analysis using these parameters. Section 3.2 provides our inter-comparison of different BC instruments using the clustering results and draws upon the statistical analysis in our interpretation. Table S2 and S3 provide all of the sample-period-integrated EF_{BC} for the different instruments as well as all fire-related parameters for each fire.

3.1. Fire-related parameters

3.1.1. Variability of parameters

Our observed MCE range from 0.80 to 0.99, with the exception of two samples collected only during later stages of smoldering combustion. These observations suggest that we collected smoke samples representative of smoldering and flaming combustion as well as a mixture of the two. The MCE range is consistent with previous field studies (e.g., 0.80 to 0.99 during BBOP (Collier et al., 2016); 0.88 to 0.94 during SEAC^{4}RS (Liu et al., 2017)) and laboratory studies (e.g., 0.85 to 0.96 during FLAME- III (May et al., 2014); 0.69 to 0.98 during FLAME-IV (Pokhrel et al., 2016)).

Figure 1a illustrates the relationship between SSA (range = 0.20 to 0.99) and MCE; SSA increases (and later plateaus) as MCE decreases, which can be attributed to a relative increase in light-scattering particulate matter emission as MCE decreases (e.g., Figure 1b). Points are colored based on our clustering analysis (see Section 3.1.2). A proposed SSA-MCE relationship at 781 nm (Liu et al., 2014) is superimposed on our data in Figure 1a; our data generally follow this predictive curve, but note the increased scatter at higher MCE, which may arise from fuel chemistry variations and the presence of non-absorbing inorganics (e.g., ammonium, nitrate, chloride) that are not well predicted by MCE (Christian et al., 2003; McMeeking et al., 2014).

The OC/EC ratio (range = 1.27 to 44.72) is also plotted against corresponding MCE in Figure 1b. The ratios are the lowest when MCE is highest (i.e., during flaming combustion), but they rapidly increase as MCE decreases. Consistent with the relationship between SSA and MCE, OC/EC ratio are lowest for flaming fires and increase with decreasing MCE.

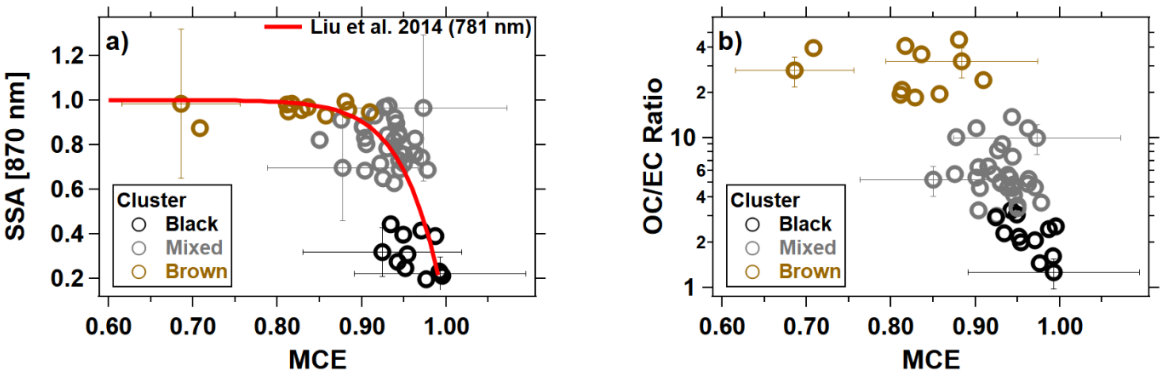

Figure 1. Sample-period-integrated SSA (a) and OC/EC ratio (b) as a function of sample-period-integrated MCE. The functional relationship between SSA (781 nm) and MCE proposed by Liu et al. (2014) is presented in panel (a) to guide the eye to the variation of SSA at higher MCE. Data points are colored by PCA/K-means clustering results. The error bars represent the propagated uncertainties calculated using the measurement uncertainties in Table 1 (The measurement uncertainties of CO_2 and CO are 0.15% and 10%, respectively).

AAE_{avg} ranged from approximately 0.97 to 2.90 for the fire sampling periods included in this work, with the highest occurring for dung emissions, which were OC-dominated (MCE ≈ 0.88, SSA ≈ 0.99, and OC/EC ≈ 45). The smallest AAE_{avg} was measured during the excelsior (wood slivers) burn, which was flaming-dominated (MCE ≈ 0.95, SSA ≈ 0.76, and OC/EC ratio ≈ 3.4). Similarly, Selimovic et al. (2018) reported an average AAE of 2.8 ± 1.57 across 31 different whole fires during the campaign (note: these measurements are mutually exclusive since the PAX-405 was shared between different projects during FIREX). Additionally, we observed similar relationships between AAE_{avg} against SSA, OC/EC ratio, and MCE as those derived from previous laboratory study (Pokhrel et al., 2016; Selimovic et al., 2018) and field measurements (Liu et al., 2014) (see Figure S9).

3.1.2. PCA/K-means clustering

MCE can be used to classify the combustion conditions during open BB into three general groups: mostly flaming combustion, mostly smoldering combustion, and a mixture of "similar" amounts of flaming and smoldering combustion (Yokelson et al., 1996). However, this classification is simple and somewhat subjective; for example Reid et al. (2005) defined flaming combustion for MCE > 0.9 and smoldering combustion for MCE < 0.9, whereas Akagi et al. (2011) defined pure flaming by MCE ~ 0.99 and pure smoldering by MCE ~ 0.8 (a fire with roughly equal contribution from flaming and smoldering would have MCE ~ 0.9). To reduce subjectivity and incorporate aerosol properties (SSA, OC/EC ratio) in our analyses, we applied PCA/K-means clustering to classify different fires using an objective statistical approach, which facilitated the comparison of different instruments.

Our PCA/K-means algorithm grouped the burns into three clusters, as shown in Figure 2a. The two PC were interim variables that reduced the dimensionality and accounted for roughly 91% of the proportions of variation in the data (74.26% and 16.70%, respectively). The K-means algorithm then used the reduced data to identify the three clusters. The clusters can be related back to the three fire-related parameters used as inputs; briefly, the three clusters were characterized as follows: (1) lower SSA and OC/EC ratio with higher MCE; (2) "mid-range" SSA, OC/EC ratio, and MCE; and (3) higher SSA and OC/EC ratio with lower MCE. One could intuitively generate similar clusters using *a priori* knowledge of BC emissions from BB, so we are able to qualitatively validate our algorithm. We will refer to Cluster (1) as "Black" (since SSA $\rightarrow$ 0 at 870 nm and median AAE_{avg} ~ 1.5), Cluster (3) as "Brown" (since SSA $\rightarrow$ 1 at 870 nm and median AAE_{avg} ~ 2.8), and Cluster (2) as "Mixed" (since these values of SSA and AAE_{avg} are somewhere in between) in order to provide each with a brief qualitative descriptor. These groupings are also included in Figure 1.

Additional clusters did not improve the quality of fit (i.e., total-WCSS = 147, 66, 25, 17, 11, and 14 for total number of the clusters (K) = 1 to 5, and an "elbow" shape was observed when K =3). Moreover, the optimized cluster number and the main characteristics within each cluster compare well with Chen et al. (2012), in which they adopted K-means on variables of SSA, AAE, MCE, and instantaneous scattering emission factor, yielding three clusters, referring as low-SSA (BC-like), high-SSA (OC-like), and intermediate in a study of biofuel emissions from cookstoves.

For further evaluation of our clustering algorithm, we used AAE_{avg} as an external criterion, shown in Figure 2b. This method was inspired by Yeung et al. (2001), in which they applied a clustering analysis to all but one experimental variable and used the remaining one to evaluate the predictive ability of the clustering. The general increase in AAE_{avg} from "Black" to "Mixed" to "Brown" followed *a priori* expectation since SSA and AAE_{avg} have been shown to be positively correlated (Liu et al., 2014; McMeeking et al., 2014; Selimovic et al., 2018). This implies that our PCA/K-means analysis is viable for clustering co-dependent BB properties on both a statistical and physical basis. Besides the association between AAE_{avg} and the three clusters, we found that the clusters appear to be related to fuel type and plant components (Figure S10). For example, most observations in the "Black" cluster are from the combustion of pine litter (e.g., dry needles) or fuels from the "chaparral" biome (e.g., manzanita, chamise). In contrast, rotten logs and "entire" fuel samples (e.g., canopy material + logs) contribute to most of the observations in the "Brown" cluster, suggesting this component produces more BrC relative

to BC. Combinations of fuel type and plant component are more distributed throughout in the "Mixed" cluster.

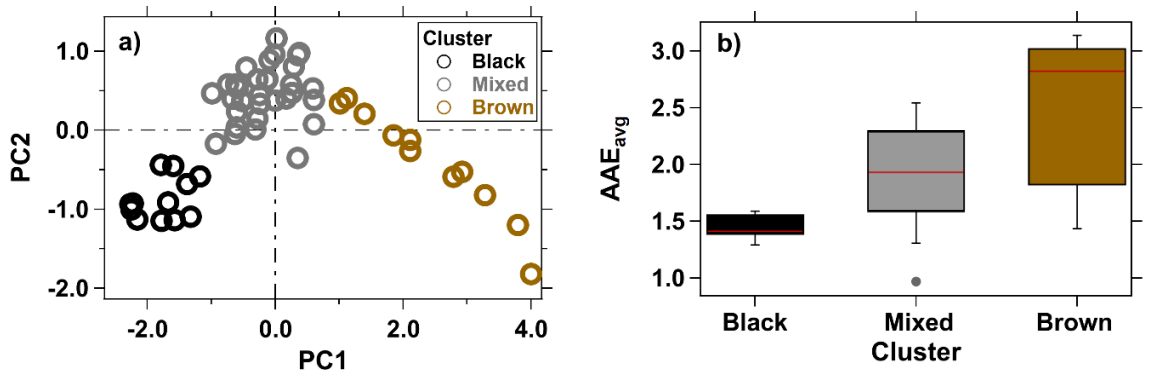

Figure 2. (a) Results of PCA/K-means clustering analysis (b) Box plot of AAE_{avg} for the different clusters.

3.2 Inter-comparison of BC measurements

3.2.1. Pairwise comparison to a reference instrument

We utilized the Bland-Altman difference approach to compare the different instruments to a reference (Figure 3; Table 2). However, as we alluded to in Section 2.4, none of the above BC instruments provided an unequivocally "ground truth" value for each experiment. We selected the PAX-870 to be the "reference" instrument in our analysis with the following rationale: (1) it was the only real-time instrument running continuously through all fires; (2) it was not constrained by size thresholds for particle detection; (3) it was relatively straightforward to calibrate; and (4) it measured light absorption *in situ* rather than after aerosol collection on a filter. Hence, for all pairs of instruments in Figure 3, the PAX-870 EF_{BC} value was the one that was subtracted in our differences. We must emphasize that it is not our intent to suggest that the PAX-870 is the "best" instrument or for the reader to infer that any of these instruments are inherently "wrong"; we provide pairwise Bland-Altman difference plots using each of the other instruments as the reference in the online Supplement (Figure S8 lower panels).

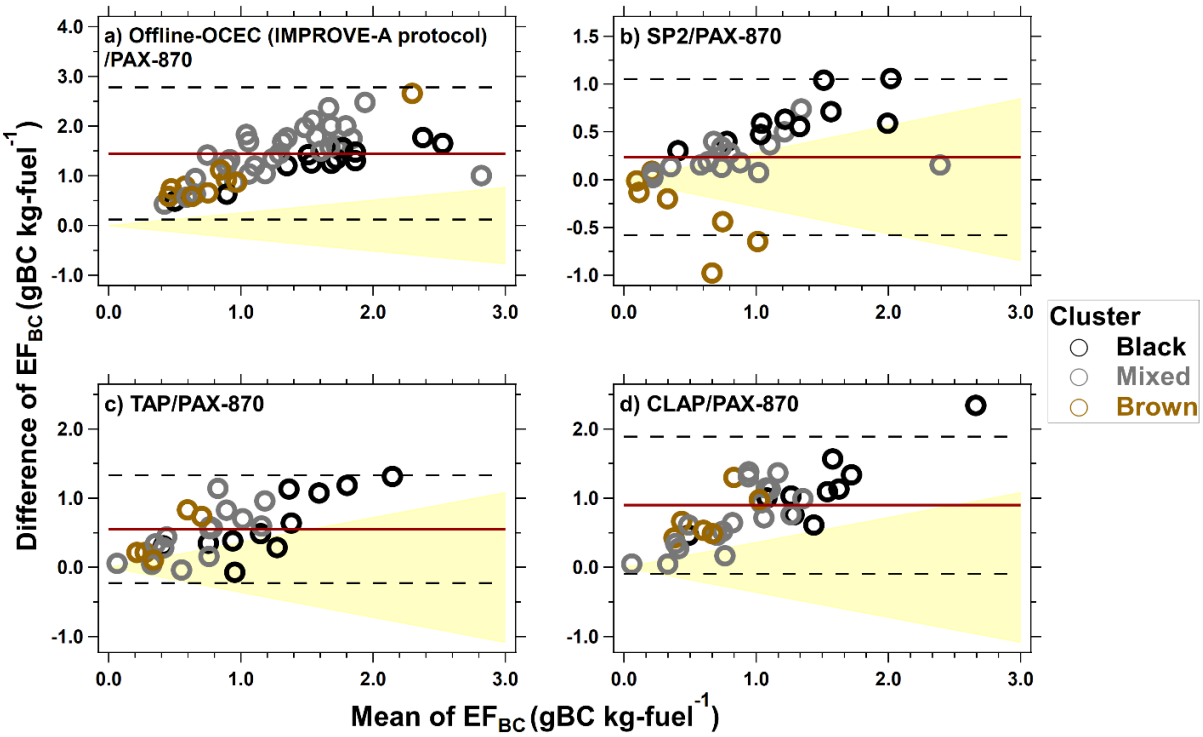

Figure 3. Bland-Altman plots for comparisons of EF_{BC} between (a) Offline OCEC (IMPROVE-A protocol)/PAX-870 (b) SP2/PAX-870 (c)TAP/PAX-870 and (d) CLAP/PAX-870. Mean difference (solid line) and limits of agreement (dashed lines) of each pair of comparison are provided in the figure. The yellow shaded region represents propagated measurement uncertainty. Note different scales for Y-axis. The Bland-Altman plot for Offline OCEC (NIOSH-870 protocol)/PAX-870 is provided in Figure S4.

Data Pair	Mean difference (95% CI) (g-BC kg-fuel^{-1})	Lower LoA (95% CI) (g-BC kg-fuel^{-1})	Upper LoA (95% CI) (g-BC kg-fuel^{-1})	Slope (Diff & Mean)	Systematic Bias?	Proportional Bias?
Offline OCEC /PAX-870	1.45 (1.26 to 1.63)	0.12 (-0.20 to 0.43)	2.78 (2.46 to 3.10)	0.83 (P<0.05)	Yes	Yes
Offline OCEC (NIOSH-870) /PAX-870	0.69 (0.59 to 0.82)	-0.22 (-0.44 to 0.01)	1.59 (1.37 to 1.81)	0.65 (P<0.05)	Yes	Yes
SP2/PAX-870	0.24 (0.09 to 0.38)	-0.58 (-0.83 to -0.33)	1.05 (0.80 to 1.30)	0.39 (P<0.05)	Yes	Yes
TAP/PAX-870	0.53 (0.40 to 0.67)	-0.23 (-0.46 to 0.01)	1.29 (1.06 to 1.52)	0.57 (P<0.05)	Yes	Yes
CLAP/PAX-870	0.87 (0.71 to 1.03)	-0.09 (-0.38 to 0.18)	1.83 (1.56 to 2.13)	0.76 (P<0.05)	Yes	Yes

Table 2. Bland-Altman statistical results

CI, confidence interval; LoA, limits of agreement (mean difference ± 1.96 × SD (standard deviation of differences). Systematic bias exists if the 95% CI of the bias does not contain zero, and proportional bias exists if the slope of the regression between difference and mean differs from zero significantly.

Overall, Figure 3 suggests that the PAX-870 generally provides a lower measurement value than the other instruments considered here but to a varying degree (as seen in the mean differences and limits of agreement in Table 2). This could imply that most instruments over-estimate BC concentrations, but it could also imply that the PAX-870 measurement is incorrect. However, in the absence of a "ground truth" measurement, we cannot confirm or reject either claim. These discrepancies between instruments cannot be explained by measurement uncertainty alone (yellow shaded areas in Figure 3 and Figure S11).

Although the PAX-870 was selected as the reference instrument, it is not without its own limitations. One cause of uncertainty in the PAX-870 measurement is related to the MAC value, which was assumed to be 4.74 m^2 g^{-1} across all eBC instruments and all fires. A central value is generally quoted with a range of ± 20% (e.g. Bond and Bergstrom (2006) gives 7.5 ± 1.2 m^2 g^{-1} at 550 nm, while Olson et al. (2015) reported lower MAC values for BB), so there is some inherent uncertainty in this value. While we could calculate MAC values using a combination of one mass-based instrument (the SP2 or offline OCEC) and one eBC instrument (PAX-870, TAP, or CLAP), this would force the instruments to agree in our comparison, which is not our intent. Another factor that could bias the PAX-870 is E_{abs} (due to the lensing effect by OC or other coating material); E_{abs} will cause the PAX-870 detect a larger eBC concentration than that from the same materials in an externally mixed form. In this work, we estimated E_{abs} to range between 1.06 and 1.96 based on SP2 analysis (typically higher values were obtained for the fires with higher SSA and OC/EC ratio). Additionally, the PAX-870 may be biased low due to potential (unquantified) losses in the dryer and scrubber. Consequently, when interpreting Figure 3 and Table 2, the potential uncertainties of the PAX-870 are equally important as those of the other four instruments.

Considering the pair of offline OCEC (IMPROVE-A)/PAX-870 (Figure 3a), the Bland-Altman approach shows that there was both a systemic bias and a proportional bias between the two instruments. The mean difference of EF_{BC} between the offline OCEC (IMPROVE-A) and PAX-870 was 1.45 ± 0.18 g-BC kg-fuel^{-1} (95% confidence interval) and did not include zero (systematic bias). The differences (y-axis) also increased from roughly 0.5 g-BC kg-fuel^{-1} to greater than 3 g-BC kg-fuel^{-1} (proportional bias; p-value of slope < 0.05). Moreover, the "cone-shaped" pattern of the data suggests that the discrepancy between the offline OCEC and PAX-870 tends to be more variable as the overall BC emissions increase (i.e., it exhibits heteroscedasticity).

Besides the aforementioned factors that may affect the PAX-870 results, the observed discrepancy between the offline OCEC and PAX-870 could be due to potential issues with the IMPROVE-A protocol when deriving EC concentration, including: (1) incomplete evolution of OC during the stage of OC analysis (Cavalli et al., 2010); (2) the OC/EC split for BB aerosols with relatively high OC/EC ratios or high OC loading on the filter (Khan et al., 2012; Wu et al., 2012); (3) the charring correction method used in the IMPROVE-A protocol (Chow et al., 2004); (4) the assumption that the PC and native EC have the same MAC in the pyrolysis correction (Chow et al., 2004; Nicolosi et al., 2018); (5) the presence of BrC and inorganic matter on the on the filters (McMeeking et al., 2009; Subramanian et al., 2007). We provide an inter-protocol comparison and discuss potential causes of the discrepancy in the supplementary text and Figure S4.

From Table 2, the SP2 and PAX-870 appear to have the best agreement based on the lowest mean difference and slope closest to zero. However, considering Figure 3b, there are two distinct trends in the data; the "Black" and "Mixed" clusters exhibit a positive proportional bias, while the "Brown" cluster exhibits a negative proportional bias. Since we report rBC after adjustments using mass correction factors, the SP2/PAX divergence is unlikely to be related to the size distribution of the samples (See SMPS-derived geometric mean diameter and geometric standard deviation in Table S2). The negative trend for the "Brown" cluster appears to be related to E_{abs}, which can shift the PAX-870 to a higher reading relative to measurements of rBC externally mixed (E_{abs} inferred from the SP2 is shown in Figure S12). On the other hand, the LII technique is less efficient in detecting small (<~0.5 fg, or approximately 70 nm VED) rBC cores when there is a significant presence of non-BC material internally mixed with the rBC (Schwarz et al., 2010). Generally, this small rBC fraction only contributes weakly (<5 %) to the accumulation mode rBC mass detected by the SP2 in biomass burning. Moreover, the SP2-derived rBC can be overestimated by laser-induced charring of organic aerosols (Sedlacek III et al., 2018). Finally, some of the differences between the SP2 and the PAX-870 could be due to the difference between the flow rates of the two instruments (PAX: 1.0 LPM, SP2: 0.006 LPM), which may result in a bias between the two instruments that we cannot identify.

The overall patterns in the Bland-Altman plots for the TAP (Figure 3c) and CLAP (Figure 3d) compared to the PAX-870 are consistent with prior work. By generating aerosol mixtures with a large range of SSA, Sheridan et al. (2005) found that the PSAP tended to slightly over-estimate the photoacoustic instrument for the particles with SSA greater than 0.67. Likewise, Arnott et al. (2003) observed that B_{abs} measured by the PSAP was roughly 60% higher than that measured by the *in situ* photoacoustic instrument during field measurements of ambient atmospheric aerosols (BC concentration <6.7 $\mu g\ m^{-3}$). These discrepancies could be due to the filter-induced biases in the measurements made by the TAP and CLAP (see Section 2.2.3 above). Even though the B1999 correction scheme is meant to address potential filter-induced biases, it was developed for PSAP using internal mixtures of ammonium sulfate and nigrosin, so it may have limitations for the BB aerosols considered in this work. Moreover, we may introduce systematic biases in our extrapolation from the original wavelengths of the filter-based instruments to 870 nm due to potential absorption by BrC at shorter wavelengths. Nevertheless, the Bland-Altman plot comparing the TAP and CLAP (Figure S8) suggests there is no proportional bias between the two filter-based instruments, and most of the discrepancy appears to be related to measurement uncertainties (Figure S12). Thus, the differences between the TAP/PAX-870 comparison (Figure 3c) and the CLAP/PAX-870 (Figure 3d) are most likely due to a combination of propagated measurement uncertainty and minor operational differences between the instruments.

Interestingly, the different clusters have slightly different behaviors within each Bland-Altman plot. We have already discussed this in the context of Figure 3b. However, considering the cone-shaped pattern in Figure 3a, the "Black" cluster mostly follows the lower boundary of the cone, while the "Brown" and "Mixed" clusters are more distributed throughout. The relatively larger uncertainty observed for the "Brown" and "Mixed" clusters could be due to a larger amount of pyrolyzed OC relative to the amount of EC present, and the detection of both PC and EC can have greater uncertainties when there is a more complicated mixture of inorganic matter on the filters (Bladt et al., 2014; Martins et al., 1998; McMeeking et al., 2009). We continue to explore these variations within and between clusters for different instruments in the next section.

3.2.2. Effect of BB properties on instrument comparisons

Due to the apparent differences between clusters in Figure 3, we explore these further here. In Figure 4, we present box-and-whisker plots of EF_{BC} ratios (using the PAX-870 in the denominator) using only the fires where data are available for each instrument in the pair. The dashed line in Figure 4 represents a ratio of 1, or perfect agreement between the two instruments. The same uncertainties discussed with respect to Figure 3 are likely applicable here as well (especially for the "Brown" and "Mixed" clusters).

Table 3 EF_{BC} derived by the five instruments across the three clusters of fires (mean ± standard deviation). Number of fires for each combination of cluster and instrument is shown in parenthesis.

Cluster	PAX-870 (g-BC kg-fuel^{-1})	Offline OCEC (IMPROVE-A) (g-BC kg-fuel^{-1})	Offline OCEC (NIOSH-870) (g-BC kg-fuel^{-1})	SP2 (g-BC kg-fuel^{-1})	TAP (g-BC kg-fuel^{-1})	CLAP (g-BC kg-fuel^{-1})
Black	0.99 ± 0.39 (n = 10)	2.27 ± 0.74 (n = 10)	1.99 ± 0.85 (n=10)	1.61 ± 0.61 (n = 10)	1.55 ± 0.69 (n = 9)	2.00 ± 0.79 (n = 8)
Mixed	0.58 ± 0.41 (n = 34)	2.11 ± 0.78 (n = 34)	1.17 ± 0.55 (n=28)	0.98 ± 0.58 (n = 15)	0.91 ± 0.45 (n = 17)	1.15 ± 0.54 (n = 19)
Brown	0.54 ± 0.42 (n = 9)	1.37 ± 0.88 (n = 11)	0.88 ± 0.35 (n=7)	0.29 ± 0.24 (n = 7)	0.62 ± 0.37 (n = 5)	1.00 ± 0.38 (n = 6)

To contextualize some of this discussion, Table 3 summarizes the EF_{BC} from each instrument for each cluster. As might be expected, the burns within the "Black" cluster have the largest EF_{BC} for each of the five instruments, and the mean EF_{BC} decreases from the "Black" to "Mixed" to "Brown" cluster. However, the trends across clusters for each instrument are not identical. For example, all values (except the offline OCEC (IMPROVE-A)) decrease by roughly 40% from the "Black" to "Mixed" clusters, but the change in EF_{BC} from the "Mixed" to "Brown" cluster is more varied (ranging from ~7% to ~70% decrease). Moreover, as suggested in the previous section, the PAX-870 consistently has the lowest EF_{BC} among all instruments for a given cluster (except for the SP2 EF_{BC} for the "Brown" cluster). Note that due to differing instrument availability throughout the campaign (e.g., the SP2 was only available during stack burns), different fires were used in the computation of the emission factors for different instruments, so a direct comparison of these EF_{BC} values (e.g., statistical significance testing) is not rigorous, but a comparison of trends is interesting..

Based on Figure 4, we make the following observations. First, by aggregating all of the ratios within each cluster, both the mean value and the range of the EF_{BC} ratios to the PAX-870 increase from the "Black" cluster (mean = 2.02, range: 0.93 to 2.92) to the "Mixed" (mean = 3.01, range: 1.05 to 8.80) to the "Brown" (mean = 3.04, range: 0.15 to 8.26). This suggests that the instruments have the best agreement for the "Black" cluster (likely chemically and optically similar to "pure" BC), and this agreement worsens for the "Mixed" and "Brown" clusters (relatively larger contributions from OC). Second, by considering different instruments across the clusters, the median EF_{BC} ratios vary from "Black" to "Mixed" to "Brown"; these values increase for the offline OC/EC (both protocols), TAP, and CLAP, and they decrease for the SP2. Third, the response of an individual instrument appears to be related to differences in aerosol optical (i.e., SSA, AAE_{avg}) and chemical (i.e., OC/EC ratio) properties, as evident in the differences between different instruments within a given cluster. All of these observations

suggest that both the measurement technique and the aerosol optical/chemical properties influence a given instrument's relative agreement with our reference instrument.

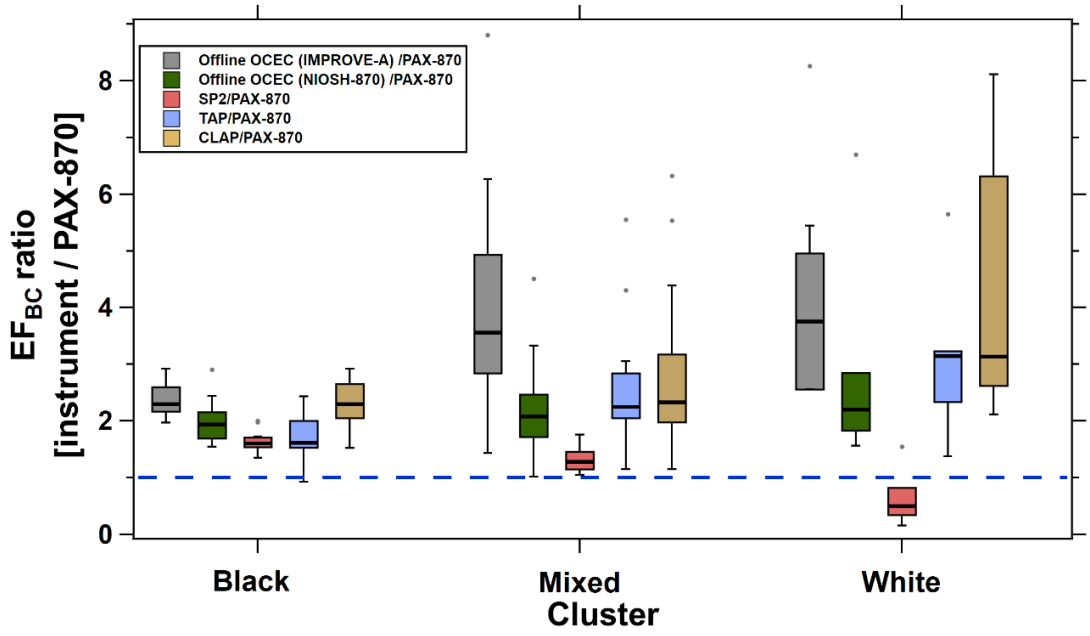

Figure 4. Box-plots for the distribution of EF_{BC} ratios (to PAX) of individual pairs of instruments across the three clusters. Within each cluster, five subgroups of EF_{BC} ratios (from left Offline OCEC (IMPROVE-A)/PAX-870, Offline OCEC (NIOSH-870)/PAX-870, SP2/PAX-870, TAP/PAX-870, and CLAP/PAX-870) are shown in different colors. The box ranges represent the lower quartile (25th percentile) and upper quartile (75th percentile) and the box height is the interquartile range (IQR). The whiskers correspond to the 10th and 90th percentiles. The line in the middle of the box represents the median, and dots represent outliers.

3.2.3. Comparison of BC from the" Black" cluster with previous studies

We have discussed some of the prior work in the Introduction, but we continue this here for context, specifically focusing on our "Black" cluster and previous laboratory studies using ethylene/air-generated soot (Cross et al., 2010; Slowik et al., 2007; Yelverton et al., 2014) and internal combustion engines (Jiang et al., 2018; Kamboures et al., 2013) since our black cluster is the cluster that is likely to be the most similar in characteristics to these sources (e.g., low SSA, low OC/EC ratio). One caveat in the comparison of our work to these prior studies is that in our "Black" cluster, the OC/EC ratio ranges from roughly 1 to 3, whereas for the ethylene/air-generated soot, the OC/EC ratio in Yelverton et al. (2014) was roughly 0.5, and for the internal combustion engines, the OC/EC ratio is likely less than one (Saliba et al., 2017); hence, directly comparing our results to these previous results may have some limitations. Another caveat is that the eBC values are used "as presented" in the various references, so the wavelength at which eBC was derived may vary and so will the wavelength-dependent MAC (Table S5), which may potentially contribute to some of the variability in that panel. In Figure 5, we present a summary of this comparison with selected previous studies that used "Black" cluster-like particles as sources. The instrument ratio in previous studies indicates the ratio of the given instrument to an

in situ eBC instrument, similar to Figure 4 (and hence, we only include those studies including *in situ* eBC measurements).

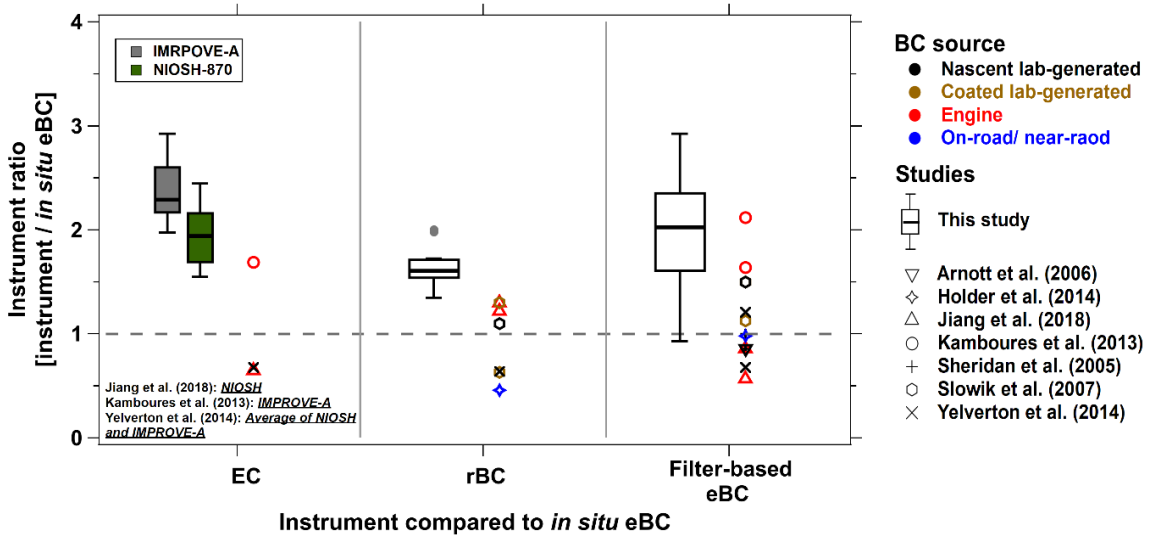

Figure 5. Instrument comparisons for "Black" cluster-like particles. Results are displayed as instrument ratios (divided by in situ eBC measurements). The line in the middle of the box represents the median of the present work.

For uncoated soot ("pure" BC), Yelverton et al. (2014) found that eBC (both filter-based and *in situ*) was roughly a factor of 1.5 greater than both rBC and EC, for which they found nearly perfect agreement. By testing BC emitted from marine engines and vehicle engines, respectively, Jiang et al. (2018) and Kamboures et al. (2013) found that different BC (excluding EC) techniques were well correlated ($R^2 > 0.85$) but had varied linear relationships (e.g. the filter-based eBC instruments provide lower values than the *in situ* eBC instrument in Jiang et al. (2018),the opposite was true in Kamboures et al. (2013)). Our EC values are higher than both our eBC and rBC values, which is consistent with Kamboures et al. (2013), but different from Jiang et al. (2018) and Yelverton et al. (2014). Compared with those studies that observed higher filter-based eBC than *in situ* eBC, our instrument ratios are similar (within a factor of 2). While the exact reason for these discrepancies is unknown, aerosol optical and chemical properties likely play a substantial role.

We can also relate our results for the "Mixed" and "Brown" clusters to prior studies. In our study, we observe a general worsening in the agreement between instrument pairs (with the exception of the SP2/PAX-870) relative to the "Black" cluster, which could be implicitly driven by aerosol optical properties. The increasing trend from "Black" to "Mixed" to "Brown" in Figure 4 is consistent with that in AAE_{avg} (Figure 2b). Similar results have been also observed in Cross et al. (2010) and Slowik et al. (2007), in which the agreement among BC instruments was worsened with the addition of organic coatings to the BC. In addition to measurement uncertainties, Reid et al. (1998) attributed discrepancies between BC instruments to highly-variable MAC, which could be affected by the presence of BrC (especially at the wavelengths of 532 nm and 550 nm that were used in that study). Hence, the presence of BrC appears to be an important source of variability in the EF_{BC} ratios, but an exhaustive comparison between our results and other studies

investigating aerosols that may fall into the "Mixed" or "Brown" clusters is outside the scope of this work.

4. Conclusions and implications

During the FIREX campaign, we conducted BC measurements using a suite of instruments, enabling an inter-comparison study for BB aerosols under a relatively wide range of fire-related parameters (MCE, SSA, OC/EC ratio, and AAE). To normalize data for different fires, time-integrated EF_{BC} for each fire were calculated for each of the five instruments. Based on the EF_{BC} results of 55 fires, the EC, rBC, and filter-based eBC were, on average, 4.7, 1.3, and 2.7 times higher, respectively, than corresponding *in situ* eBC, which was selected as the reference instrument; the majority of these differences do not appear to be attributable to measurement uncertainty alone (Figure S11).

To further interpret our data, we utilized a PCA/K-means clustering approach, which resulted in three clusters. The cluster that was the most optically similar to "pure" BC (mean SSA = 0.31 and AAE = 1.44) exhibited the greatest agreement between instruments (Figure 4); comparing our results to prior work indicated that our comparisons of EC, rBC, and filter-based eBC to *in situ* eBC were relatively similar to what others have observed previously (Figure 5). As the BB aerosols became more reflective (i.e., as SSA increased) and browner (i.e., as AAE increased), the agreement between the instruments worsened (Figure 4).

Consequently, we have several suggestions regarding data collection and data interpretation that will facilitate future comparisons of BC data collected by different instruments and from different fires:

Data Collection

- Optical and chemical properties appear to play a role in measurements of both eBC and EC for BB aerosol, but this does not seem to apply to rBC based on our data. Regardless, we recommend reporting values of SSA, AAE, and OC/EC ratio (or equivalent, e.g., OA/rBC ratio) when reporting EF_{BC} when possible or estimating those parameters from MCE as in Figure 1 and Figure S9.
- Correction schemes for filter-based methods may require further evaluation to determine their applicability to BB aerosols.
- Heating samples to reduce the influence of coating materials prior to sampling may provide estimates of EF_{BC} for BB with the lowest uncertainty (as long as the charring of the coating material is minimal).

Data Interpretation

- Care should be taken when merging EF_{BC} data sets generated using different measurement techniques to distinguish between natural variability and instrument differences.
    - The relative standard deviation for a given cluster and given BC instrument ranges from roughly 30-80% (based on Table 3). Moreover, the relative decrease of EF_{BC} from "Black" to the "Brown" for each instrument spans the ranges from roughly 40% to 80% (also based on Table 3). While these numbers appear to be somewhat large,

    - they represent natural variability, or simply, differences in emissions between different fires. When interpreting data, we consider this a “true” uncertainty.
    - The challenge arises for instrument differences, which we consider a “false” uncertainty. For example, the median EF_{BC} ratios range from roughly 0.5 to 3.5 (Figure 4). While this range falls within the range of natural variability, the data we present here represents 55 fires. Because emission inventories are typically based on averaging field observations (e.g., Akagi et al., (2011)), developing such an inventory by combining eBC, EC, and rBC data collected for different fires may artificially inflate the uncertainty associated with EF_{BC}. This may become especially important as “historic” EC-based EF_{BC} are combined with more recent rBC-based EF_{BC}.
- Agreement between instruments is best for the “Black” cluster, which is likely to be the most similar (chemically and optically) to “pure” BC (with limited contribution from OC). This “Black” cluster may be representative of some smoke plumes in the real world. However, most ambient BB smoke plumes are likely more similar to the “Mixed” or “Brown” clusters. This will become especially problematic when the smoke undergoes photochemical aging and/or mixing with other air masses, so BC measurements from the same fire may vary with smoke age (e.g., Akagi et al., (2012); Yokelson et al., (2009)).
- An empirical absorption EF, which does not require the assignment of MAC, may work best in some cases for light absorption instruments (e.g., Selimovic et al., (2018) and references therein).

Data availability

Raw data are freely available from https://esrl.noaa.gov/csd/project/firex.

Acknowledgements

HL, GRM, and AAM were supported by NOAA Climate Program Office Grant NA16OAR4310109. VS and RJY were supported by NOAA Climate Program Office Grant NA16OAR4310100. Purchase of the PAX-405 was supported by NSF grant AGS-1349976. Indonesian peat fuel was provided through NASA grant NNX14AP46G-ACCDAM to the University of Montana. The authors acknowledge Pat Sheridan, John Ogren, and Derek Hageman at NOAA for loaning us the CLAP and processing data, and we thank Pat Sheridan and Fred Brechtel for useful discussions. We thank Tony Prenni from the National Park Service for lending us the AE31. We thank Nick Good from Colorado State University for his help during the campaign. We thank Jim Roberts and Carsten Warneke from NOAA for their contributions in organizing the FIREX campaign and the USDA Fire Sciences Lab personnel for their assistance and cooperation during the campaign. Olivia Ambuehl provided assistance with the OC/EC analysis.

References

Ajtai, T., Filep, Á., Utry, N., Schnaiter, M., Linke, C., Bozóki, Z., Szabó, G. and Leisner, T.: Inter-comparison of optical absorption coefficients of atmospheric aerosols determined by a multi-wavelength photoacoustic spectrometer and an Aethalometer under sub-urban wintry conditions, J. Aerosol Sci., 42(12), 859–866, doi:10.1016/j.jaerosci.2011.07.008, 2011.

Akagi, S. K., Yokelson, R. J., Wiedinmyer, C., Alvarado, M. J., Reid, J. S., Karl, T., Crounse, J. D. and Wennberg, P. O.: Emission factors for open and domestic biomass burning for use in atmospheric models, Atmos. Chem. Phys., 11(9), 4039–4072, doi:10.5194/acp-11-4039-2011, 2011.

Akagi, S. K., Craven, J. S., Taylor, J. W., McMeeking, G. R., Yokelson, R. J., Burling, I. R., Urbanski, S. P., Wold, C. E., Seinfeld, J. H., Coe, H., Alvarado, M. J. and Weise, D. R.: Evolution of trace gases and particles emitted by a chaparral fire in California, Atmos. Chem. Phys., 12(3), 1397–1421, doi:10.5194/acp-12-1397-2012, 2012.

Arnott, W. P., Moosmüller, H., Sheridan, P. J., Ogren, J. A., Raspet, R., Slaton, W. V., Hand, J. L., Kreidenweis, S. M. and Collett, J. L.: Photoacoustic and filter-based ambient aerosol light absorption measurements: Instrument comparisons and the role of relative humidity, J. Geophys. Res., 108(D1), 4034, doi:10.1029/2002JD002165, 2003.

Backman, J., Virkkula, A., Vakkari, V., Beukes, J. P., Van Zyl, P. G., Josipovic, M., Piketh, S., Tiitta, P., Chiloane, K., Petäjä, T., Kulmala, M. and Laakso, L.: Differences in aerosol absorption Ångström exponents between correction algorithms for a particle soot absorption photometer measured on the South African Highveld, Atmos. Meas. Tech., 7(12), 4285–4298, doi:10.5194/amt-7-4285-2014, 2014.

Birch, M. E. and Cary, R. A.: Elemental Carbon-Based Method for Monitoring Occupational Exposures to Particulate Diesel Exhaust, Aerosol Sci. Technol., 25(3), 221–241, doi:10.1080/02786829608965393, 1996.

Bladt, H., Ivleva, N. P. and Niessner, R.: Internally mixed multicomponent soot: Impact of different salts on soot structure and thermo-chemical properties, J. Aerosol Sci., 70, 26–35, doi:10.1016/j.jaerosci.2013.11.007, 2014.

Bond, T. C. and Bergstrom, R. W.: Light absorption by carbonaceous particles: An investigative review, Aerosol Sci. Technol., 40(1), 27–67, doi:10.1080/02786820500421521, 2006.

Bond, T. C., Anderson, T. L. and Campbell, D.: Calibration and Intercomparison of Filter-Based Measurements of Visible Light Absorption by Aerosols, Aerosol Sci. Technol., 30(6), 582–600, doi:10.1080/027868299304435, 1999.

811 Bond, T. C., Habib, G. and Bergstrom, R. W.: Limitations in the enhancement of visible light
812 absorption due to mixing state, J. Geophys. Res., 111(D20), D20211,
813 doi:10.1029/2006JD007315, 2006.

814 Bond, T. C., Doherty, S. J., Fahey, D. W., Forster, P. M., Berntsen, T., Deangelo, B. J., Flanner,
815 M. G., Ghan, S., Kärcher, B., Koch, D., Kinne, S., Kondo, Y., Quinn, P. K., Sarofim, M. C.,
816 Schultz, M. G., Schulz, M., Venkataraman, C., Zhang, H., Zhang, S., Bellouin, N., Guttikunda, S.
817 K., Hopke, P. K., Jacobson, M. Z., Kaiser, J. W., Klimont, Z., Lohmann, U., Schwarz, J. P.,
818 Shindell, D., Storelvmo, T., Warren, S. G. and Zender, C. S.: Bounding the role of black carbon
819 in the climate system: A scientific assessment, J. Geophys. Res. Atmos., 118(11), 5380–5552,
820 doi:10.1002/jgrd.50171, 2013.

821 Cappa, C. D., Onasch, T. B., Massoli, P., Worsnop, D. R., Bates, T. S., Cross, E. S., Davidovits,
822 P., Hakala, J., Hayden, K. L., Jobson, B. T., Kolesar, K. R., Lack, D. A., Lerner, B. M., Li, S. M.,
823 Mellon, D., Nuaaman, I., Olfert, J. S., Petäjä, T., Quinn, P. K., Song, C., Subramanian, R.,
824 Williams, E. J. and Zaveri, R. A.: Radiative absorption enhancements due to the mixing state of
825 atmospheric black carbon, Science (80-.)., 337(6098), 1078–1081, doi:10.1126/science.1223447,
826 2012.

827 Chen, Y., Roden, C. A. and Bond, T. C.: Characterizing Biofuel Combustion with Patterns of
828 Real-Time Emission Data (PaRTED), Environ. Sci. Technol., 46(11), 6110–6117,
829 doi:10.1021/es3003348, 2012.

830 Cheng, Y., Duan, F., He, K., Zheng, M., Du, Z., Ma, Y. and Tan, J.: Intercomparison of
831 Thermal–Optical Methods for the Determination of Organic and Elemental Carbon: Influences
832 of Aerosol Composition and Implications, Environ. Sci. Technol., 45(23), 10117–10123,
833 doi:10.1021/es202649g, 2011.

834 Chow, J. C., Watson, J. G., Pritchett, L. C., Pierson, W. R., Frazier, C. A. and Purcell, R. G.: The
835 dri thermal/optical reflectance carbon analysis system: description, evaluation and applications in
836 U.S. Air quality studies, Atmos. Environ. Part A. Gen. Top., 27(8), 1185–1201,
837 doi:10.1016/0960-1686(93)90245-T, 1993.

838 Chow, J. C., Watson, J. G., Chen, L.-W. A., Arnott, W. P., Moosmüller, H. and Fung, K.:
839 Equivalence of Elemental Carbon by Thermal/Optical Reflectance and Transmittance with
840 Different Temperature Protocols, Environ. Sci. Technol., 38(16), 4414–4422,
841 doi:10.1021/es034936u, 2004.

842 Christian, T. J., Kleiss, B., Yokelson, R. J., Holzinger, R., Crutzen, P. J., Hao, W. M., Saharjo;, B.
843 H. and Ward, D. E.: Comprehensive laboratory measurements of biomass-burning emissions: 1.
844 Emissions from Indonesian, African, and other fuels, J. Geophys. Res., 108(D23), 4719,
845 doi:10.1029/2003JD003704, 2003.

Clarke, A., McNaughton, C., Kapustin, V., Shinozuka, Y., Howell, S., Dibb, J., Zhou, J., Anderson, B., Brekhovskikh, V., Turner, H. and Pinkerton, M.: Biomass burning and pollution aerosol over North America: Organic components and their influence on spectral optical properties and humidification response, J. Geophys. Res., 112(D12), D12S18, doi:10.1029/2006JD007777, 2007.

Collier, S., Zhou, S., Onasch, T. B., Jaffe, D. A., Kleinman, L., Sedlacek, A. J., Briggs, N. L., Hee, J., Fortner, E., Shilling, J. E., Worsnop, D., Yokelson, R. J., Parworth, C., Ge, X., Xu, J., Butterfield, Z., Chand, D., Dubey, M. K., Pekour, M. S., Springston, S. and Zhang, Q.: Regional Influence of Aerosol Emissions from Wildfires Driven by Combustion Efficiency: Insights from the BBOP Campaign, Environ. Sci. Technol., 50(16), 8613–8622, doi:10.1021/acs.est.6b01617, 2016.

Cross, E. S., Onasch, T. B., Ahern, A., Wrobel, W., Slowik, J. G., Olfert, J., Lack, D. A., Massoli, P., Cappa, C. D., Schwarz, J. P., Spackman, J. R., Fahey, D. W., Sedlacek, A., Trimborn, A., Jayne, J. T., Freedman, A., Williams, L. R., Ng, N. L., Mazzoleni, C., Dubey, M., Brem, B., Kok, G., Subramanian, R., Freitag, S., Clarke, A., Thornhill, D., Marr, L. C., Kolb, C. E., Worsnop, D. R. and Davidovits, P.: Soot particle studies-instrument inter-comparison-project overview, Aerosol Sci. Technol., 44(8), 592–611, doi:10.1080/02786826.2010.482113, 2010.

Fierce, L., Bond, T. C., Bauer, S. E., Mena, F. and Riemer, N.: Black carbon absorption at the global scale is affected by particle-scale diversity in composition, Nat. Commun., 7, 12361, doi:10.1038/ncomms12361, 2016.

Fuller, K. A., Malm, W. C. and Kreidenweis, S. M.: Effects of mixing on extinction by carbonaceous particles, J. Geophys. Res. Atmos., 104(D13), 15941–15954, doi:10.1029/1998JD100069, 1999.

Gao, R. S., Schwarz, J. P., Kelly, K. K., Fahey, D. W., Watts, L. A., Thompson, T. L., Spackman, J. R., Slowik, J. G., Cross, E. S., Han, J.-H., Davidovits, P., Onasch, T. B. and Worsnop, D. R.: A Novel Method for Estimating Light-Scattering Properties of Soot Aerosols Using a Modified Single-Particle Soot Photometer, Aerosol Sci. Technol., 41(2), 125–135, doi:10.1080/02786820601118398, 2007.

Hardy, A.: An examination of procedures for determining the number of clusters in a data set, in New Approaches in Classification and Data Analysis, pp. 178–185, Springer, Berlin, Heidelberg., 1994.

Hartigan, J. A. and Wong, M. A.: Algorithm AS 136: A K-Means Clustering Algorithm, Appl. Stat., 28(1), 100, doi:10.2307/2346830, 1979.

Hitzenberger, R., Petzold, A., Bauer, H., Ctyroky, P., Pouresmaeil, P., Laskus, L. and Puxbaum, H.: Intercomparison of Thermal and Optical Measurement Methods for Elemental Carbon and

881 Black Carbon at an Urban Location, Environ. Sci. Technol., 40(20), 6377–6383,
882 doi:10.1021/es051228v, 2006.

883 Holder, A. L., Hagler, G. S. W., Yelverton, T. L. B. and Hays, M. D.: On-road black carbon
884 instrument intercomparison and aerosol characteristics by driving environment, Atmos. Environ.,
885 88, 183–191, doi:10.1016/j.atmosenv.2014.01.021, 2014.

886 Hosseini, S., Urbanski, S. P., Dixit, P., Qi, L., Burling, I. R., Yokelson, R. J., Johnson, T. J.,
887 Shrivastava, M., Jung, H. S., Weise, D. R., Miller, J. W. and Cocker, D. R.: Laboratory
888 characterization of PM emissions from combustion of wildland biomass fuels, J. Geophys. Res.
889 Atmos., 118(17), 9914–9929, doi:10.1002/jgrd.50481, 2013.

890 Jacobson, M. Z.: A physically-based treatment of elemental carbon optics: Implications for
891 global direct forcing of aerosols, Geophys. Res. Lett., 27(2), 217–220,
892 doi:10.1029/1999GL010968, 2000.

893 Jeong, C. H., Hopke, P. K., Kim, E. and Lee, D. W.: The comparison between thermal-optical
894 transmittance elemental carbon and Aethalometer black carbon measured at multiple monitoring
895 sites, Atmos. Environ., 38(31), 5193–5204, doi:10.1016/j.atmosenv.2004.02.065, 2004.

896 Jiang, Y., Yang, J., Gagné, S., Chan, T. W., Thomson, K., Fofie, E., Cary, R. A., Rutherford, D.,
897 Comer, B., Swanson, J., Lin, Y., Van Rooy, P., Asa-Awuku, A., Jung, H., Barsanti, K.,
898 Karavalakis, G., Cocker, D., Durbin, T. D., Miller, J. W. and Johnson, K. C.: Sources of variance
899 in BC mass measurements from a small marine engine: Influence of the instruments, fuels and
900 loads, Atmos. Environ., 182, 128–137, doi:10.1016/j.atmosenv.2018.03.008, 2018.

901 Jolliffe, I. T.: Principal Component Analysis and Factor Analysis, in Principal component
902 analysis, pp. 115–128., 1986.

903 Kamboures, M. A., Hu, S., Yu, Y., Sandoval, J., Rieger, P., Huang, S.-M., Zhang, S., Dzhema, I.,
904 Huo, D., Ayala, A. and Chang, M. C. O.: Black carbon emissions in gasoline vehicle exhaust: A
905 measurement and instrument comparison, J. Air Waste Manage. Assoc., 63(8), 886–901,
906 doi:10.1080/10962247.2013.787130, 2013.

907 Khan, B., Hays, M. D., Geron, C. and Jetter, J.: Differences in the OC/EC Ratios that
908 Characterize Ambient and Source Aerosols due to Thermal-Optical Analysis, Aerosol Sci.
909 Technol., 46(2), 127–137, doi:10.1080/02786826.2011.609194, 2012.

910 Kirchstetter, T. W., Novakov, T. and Hobbs, P. V.: Evidence that the spectral dependence of
911 light absorption by aerosols is affected by organic carbon, J. Geophys. Res. Atmos., 109(D21),
912 n/a-n/a, doi:10.1029/2004JD004999, 2004.

913 Kondo, Y., Matsui, H., Moteki, N., Sahu, L., Takegawa, N., Kajino, M., Zhao, Y., Cubison, M. J.,
914 Jimenez, J. L., Vay, S., Diskin, G. S., Anderson, B., Wisthaler, A., Mikoviny, T., Fuelberg, H. E.,
915 Blake, D. R., Huey, G., Weinheimer, A. J., Knapp, D. J. and Brune, W. H.: Emissions of black
916 carbon, organic, and inorganic aerosols from biomass burning in North America and Asia in
917 2008, J. Geophys. Res., 116(D8), D08204, doi:10.1029/2010JD015152, 2011.

918 Koss, A. R., Sekimoto, K., Gilman, J. B., Selimovic, V., Coggon, M. M., Zarzana, K. J., Yuan,
919 B., Lerner, B. M., Brown, S. S., Jimenez, J. L., Krechmer, J., Roberts, J. M., Warneke, C.,
920 Yokelson, R. J. and de Gouw, J.: Non-methane organic gas emissions from biomass burning:
921 identification, quantification, and emission factors from PTR-ToF during the FIREX 2016
922 laboratory experiment, Atmos. Chem. Phys., 18(5), 3299–3319, doi:10.5194/acp-18-3299-2018,
923 2018.

924 de la Sota, C., Kane, M., Mazorra, J., Lumbreras, J., Youm, I. and Viana, M.: Intercomparison of
925 methods to estimate black carbon emissions from cookstoves, Sci. Total Environ., 595, 886–893,
926 doi:10.1016/j.scitotenv.2017.03.247, 2017.

927 Laborde, M., Mertes, P., Zieger, P., Dommen, J., Baltensperger, U. and Gysel, M.: Sensitivity of
928 the Single Particle Soot Photometer to different black carbon types, Atmos. Meas. Tech., 5(5),
929 1031–1043, doi:10.5194/amt-5-1031-2012, 2012a.

930 Laborde, M., Schnaiter, M., Linke, C., Saathoff, H., Naumann, K.-H., Möhler, O., Berlenz, S.,
931 Wagner, U., Taylor, J. W., Liu, D., Flynn, M., Allan, J. D., Coe, H., Heimerl, K., Dahlkötter, F.,
932 Weinzierl, B., Wollny, A. G., Zanatta, M., Cozic, J., Laj, P., Hitzenberger, R., Schwarz, J. P. and
933 Gysel, M.: Single Particle Soot Photometer intercomparison at the AIDA chamber, Atmos. Meas.
934 Tech., 5(12), 3077–3097, doi:10.5194/amt-5-3077-2012, 2012b.

935 Lack, D. A. and Cappa, C. D.: Impact of brown and clear carbon on light absorption
936 enhancement, single scatter albedo and absorption wavelength dependence of black carbon,
937 Atmos. Chem. Phys., 10(9), 4207–4220, doi:10.5194/acp-10-4207-2010, 2010.

938 Lack, D. A. and Langridge, J. M.: On the attribution of black and brown carbon light absorption
939 using the Ångström exponent, Atmos. Chem. Phys., 13(20), 10535–10543, doi:10.5194/acp-13-
940 10535-2013, 2013.

941 Lack, D. A., Cappa, C. D., Covert, D. S., Baynard, T., Massoli, P., Sierau, B., Bates, T. S., Quinn,
942 P. K., Lovejoy, E. R. and Ravishankara, A. R.: Bias in Filter-Based Aerosol Light Absorption
943 Measurements Due to Organic Aerosol Loading: Evidence from Ambient Measurements,
944 Aerosol Sci. Technol., 42(12), 1033–1041, doi:10.1080/02786820802389277, 2008.

945 Lack, D. A., Moosmüller, H., McMeeking, G. R., Chakrabarty, R. K. and Baumgardner, D.:
946 Characterizing elemental, equivalent black, and refractory black carbon aerosol particles: A
947 review of techniques, their limitations and uncertainties, Anal. Bioanal. Chem., 406(1), 99–122,

948 doi:10.1007/s00216-013-7402-3, 2014.

949 Laing, J. R., Jaffe, D. A. and Hee, J. R.: Physical and optical properties of aged biomass burning
950 aerosol from wildfires in Siberia and the Western USA at the Mt. Bachelor Observatory, Atmos.
951 Chem. Phys., 16(23), 15185–15197, doi:10.5194/acp-16-15185-2016, 2016.

952 Liousse, C., Cachier, H. and Jennings, S. G.: Optical and thermal measurements of black carbon
953 aerosol content in different environments: Variation of the specific attenuation cross-section,
954 sigma (σ), Atmos. Environ. Part A. Gen. Top., 27(8), 1203–1211, 1993.

955 Liu, J., Bergin, M., Guo, H., King, L., Kotra, N., Edgerton, E. and Weber, R. J.: Size-resolved
956 measurements of brown carbon in water and methanol extracts and estimates of their
957 contribution to ambient fine-particle light absorption, Atmos. Chem. Phys., 13(24), 12389–12404,
958 doi:10.5194/acp-13-12389-2013, 2013.

959 Liu, S., Aiken, A. C., Arata, C., Dubey, M. K., Stockwell, C. E., Yokelson, R. J., Stone, E. A.,
960 Jayarathne, T., Robinson, A. L., DeMott, P. J. and Kreidenweis, S. M.: Aerosol single scattering
961 albedo dependence on biomass combustion efficiency: Laboratory and field studies, Geophys.
962 Res. Lett., 41(2), 742–748, doi:10.1002/2013GL058392, 2014.

963 Liu, X., Huey, L. G., Yokelson, R. J., Selimovic, V., Simpson, I. J., Müller, M., Jimenez, J. L.,
964 Campuzano-Jost, P., Beyersdorf, A. J., Blake, D. R., Butterfield, Z., Choi, Y., Crounse, J. D.,
965 Day, D. A., Diskin, G. S., Dubey, M. K., Fortner, E., Hanisco, T. F., Hu, W., King, L. E.,
966 Kleinman, L., Meinardi, S., Mikoviny, T., Onasch, T. B., Palm, B. B., Peischl, J., Pollack, I. B.,
967 Ryerson, T. B., Sachse, G. W., Sedlacek, A. J., Shilling, J. E., Springston, S., St. Clair, J. M.,
968 Tanner, D. J., Teng, A. P., Wennberg, P. O., Wisthaler, A. and Wolfe, G. M.: Airborne
969 measurements of western U.S. wildfire emissions: Comparison with prescribed burning and air
970 quality implications, J. Geophys. Res., 122(11), 6108–6129, doi:10.1002/2016JD026315, 2017.

971 Ludbrook, J.: Linear regression analysis for comparing two measurers or methods of
972 measurement: But which regression?, Clin. Exp. Pharmacol. Physiol., 37(7), 692–699,
973 doi:10.1111/j.1440-1681.2010.05376.x, 2010.

974 Martins, J. V., Artaxo, P., Liousse, C., Reid, J. S., Hobbs, P. V. and Kaufman, Y. J.: Effects of
975 black carbon content, particle size, and mixing on light absorption by aerosols from biomass
976 burning in Brazil, J. Geophys. Res. Atmos., 103(D24), 32041–32050, doi:10.1029/98JD02593,
977 1998.

978 May, A. A., McMeeking, G. R., Lee, T., Taylor, J. W., Craven, J. S., Burling, I., Sullivan, A. P.,
979 Akagi, S., Collett, J. L., Flynn, M., Coe, H., Urbanski, S. P., Seinfeld, J. H., Yokelson, R. J. and
980 Kreidenweis, S. M.: Aerosol emissions from prescribed fires in the United States: A synthesis of
981 laboratory and aircraft measurements, J. Geophys. Res. Atmos., 119(20), 11,826-11,849,
982 doi:10.1002/2014JD021848, 2014.

McMeeking, G. R., Kreidenweis, S. M., Baker, S., Carrico, C. M., Chow, J. C., Collett, J. L., Hao, W. M., Holden, A. S., Kirchstetter, T. W., Malm, W. C., Moosmüller, H., Sullivan, A. P. and Cyle E., W.: Emissions of trace gases and aerosols during the open combustion of biomass in the laboratory, J. Geophys. Res. Atmos., 114(19), 1–20, doi:10.1029/2009JD011836, 2009.

McMeeking, G. R., Fortner, E., Onasch, T. B., Taylor, J. W., Flynn, M., Coe, H. and Kreidenweis, S. M.: Impacts of nonrefractory material on light absorption by aerosols emitted from biomass burning, J. Geophys. Res. Atmos., 119(21), 12,272-12,286, doi:10.1002/2014JD021750, 2014.

Miyakawa, T., Kanaya, Y., Komazaki, Y., Taketani, F., Pan, X., Irwin, M. and Symonds, J.: Intercomparison between a single particle soot photometer and evolved gas analysis in an industrial area in Japan: Implications for the consistency of soot aerosol mass concentration measurements, Atmos. Environ., 127, 14–21, doi:10.1016/j.atmosenv.2015.12.018, 2016.

Moteki, N. and Kondo, Y.: Dependence of Laser-Induced Incandescence on Physical Properties of Black Carbon Aerosols: Measurements and Theoretical Interpretation, Aerosol Sci. Technol., 44(8), 663–675, doi:10.1080/02786826.2010.484450, 2010.

Moteki, N., Kondo, Y. and Nakamura, S.: Method to measure refractive indices of small nonspherical particles: Application to black carbon particles, J. Aerosol Sci., 41(5), 513–521, doi:10.1016/j.jaerosci.2010.02.013, 2010.

Müller, T., Henzing, J. S., de Leeuw, G., Wiedensohler, A., Alastuey, A., Angelov, H., Bizjak, M., Collaud Coen, M., Engström, J. E., Gruening, C., Hillamo, R., Hoffer, A., Imre, K., Ivanow, P., Jennings, G., Sun, J. Y., Kalivitis, N., Karlsson, H., Komppula, M., Laj, P., Li, S.-M., Lunder, C., Marinoni, A., Martins dos Santos, S., Moerman, M., Nowak, A., Ogren, J. A., Petzold, A., Pichon, J. M., Rodriquez, S., Sharma, S., Sheridan, P. J., Teinilä, K., Tuch, T., Viana, M., Virkkula, A., Weingartner, E., Wilhelm, R. and Wang, Y. Q.: Characterization and intercomparison of aerosol absorption photometers: result of two intercomparison workshops, Atmos. Meas. Tech., 4(2), 245–268, doi:10.5194/amt-4-245-2011, 2011.

Murphy, D. M.: The Effect of Water Evaporation on Photoacoustic Signals in Transition and Molecular Flow, Aerosol Sci. Technol., 43(4), 356–363, doi:10.1080/02786820802657392, 2009.

Nakayama, T., Suzuki, H., Kagamitani, S., Ikeda, Y., Uchiyama, A. and Matsumi, Y.: Characterization of a Three Wavelength Photoacoustic Soot Spectrometer (PASS-3) and a Photoacoustic Extinctiometer (PAX), J. Meteorol. Soc. Japan. Ser. II, 93(2), 285–308, doi:10.2151/jmsj.2015-016, 2015.

Nieuwenhuijsen, M. J., Donaire-Gonzalez, D., Rivas, I., De Castro, M., Cirach, M., Hoek, G., Seto, E., Jerrett, M. and Sunyer, J.: Variability in and agreement between modeled and personal continuously measured black carbon levels using novel smartphone and sensor technologies,

Environ. Sci. Technol., 49(5), 2977–2982, doi:10.1021/es505362x, 2015.

Ogren, J. A.: Comment on " Calibration and Intercomparison of Filter-Based Measurements of Visible Light Absorption by Aerosols " Comment on " Calibration and Intercomparison of Filter-Based Measurements of Visible Light Absorption by Aerosols ," Aerosol Sci. Technol., 44(December), 589–591, doi:10.1080/02786826.2010.482111, 2010.

Ogren, J. A., Wendell, J., Andrews, E. and Sheridan, P. J.: Continuous light absorption photometer for long-term studies, Atmos. Meas. Tech., 10(12), 4805–4818, doi:10.5194/amt-10-4805-2017, 2017.

Olson, M. R., Victoria Garcia, M., Robinson, M. A., Van Rooy, P., Dietenberger, M. A., Bergin, M. and Schauer, J. J.: Investigation of black and brown carbon multiple-wavelength-dependent light absorption from biomass and fossil fuel combustion source emissions, J. Geophys. Res. Atmos., 120(13), 6682–6697, doi:10.1002/2014JD022970, 2015.

Petzold, A., Ogren, J. A., Fiebig, M., Laj, P., Li, S. M., Baltensperger, U., Holzer-Popp, T., Kinne, S., Pappalardo, G., Sugimoto, N., Wehrli, C., Wiedensohler, A. and Zhang, X. Y.: Recommendations for reporting black carbon measurements, Atmos. Chem. Phys., 13(16), 8365–8379, doi:10.5194/acp-13-8365-2013, 2013.

Pokhrel, R. P., Wagner, N. L., Langridge, J. M., Lack, D. A., Jayarathne, T., Stone, E. A., Stockwell, C. E., Yokelson, R. J. and Murphy, S. M.: Parameterization of single-scattering albedo (SSA) and absorption Ångström exponent (AAE) with EC/OC for aerosol emissions from biomass burning, Atmos. Chem. Phys., 16(15), 9549–9561, doi:10.5194/acp-16-9549-2016, 2016.

Reid, J. S., Hobbs, P. V., Liousse, C., Martins, J. V., Weiss, R. E. and Eck, T. F.: Comparisons of techniques for measuring shortwave absorption and black carbon content of aerosols from biomass burning in Brazil, J. Geophys. Res. Atmos., 103(D24), 32031–32040, doi:10.1029/98JD00773, 1998.

Reid, J. S., Koppmann, R., Eck, T. F. and Eleuterio, D. P.: A review of biomass burning emissions part II: intensive physical properties of biomass burning particles, Atmos. Chem. Phys., 5(3), 799–825, doi:10.5194/acp-5-799-2005, 2005.

Reisinger, P., Wonaschütz, A., Hitzenberger, R., Petzold, A., Bauer, H., Jankowski, N., Puxbaum, H., Chi, X. and Maenhaut, W.: Intercomparison of Measurement Techniques for Black or Elemental Carbon Under Urban Background Conditions in Wintertime: Influence of Biomass Combustion, Environ. Sci. Technol., 42(3), 884–889, doi:10.1021/es0715041, 2008.

Ryan, T. P. and Woodall, W. H.: The most-cited statistical papers, J. Appl. Stat., 32(5), 461–474,

1051 doi:10.1080/02664760500079373, 2005.

1052 Saliba, G., Saleh, R., Zhao, Y., Presto, A. A., Lambe, A. T., Frodin, B., Sardar, S., Maldonado,
1053 H., Maddox, C., May, A. A., Drozd, G. T., Goldstein, A. H., Russell, L. M., Hagen, F. and
1054 Robinson, A. L.: Comparison of Gasoline Direct-Injection (GDI) and Port Fuel Injection (PFI)
1055 Vehicle Emissions: Emission Certification Standards, Cold-Start, Secondary Organic Aerosol
1056 Formation Potential, and Potential Climate Impacts, Environ. Sci. Technol., 51(11), 6542–6552,
1057 doi:10.1021/acs.est.6b06509, 2017.

1058 Schwarz, J. P., Gao, R. S., Fahey, D. W., Thomson, D. S., Watts, L. A., Wilson, J. C., Reeves, J.
1059 M., Darbeheshti, M., Baumgardner, D. G., Kok, G. L., Chung, S. H., Schulz, M., Hendricks, J.,
1060 Lauer, A., Kärcher, B., Slowik, J. G., Rosenlof, K. H., Thompson, T. L., Langford, A. O.,
1061 Loewenstein, M. and Aikin, K. C.: Single-particle measurements of midlatitude black carbon and
1062 light-scattering aerosols from the boundary layer to the lower stratosphere, J. Geophys. Res.,
1063 111(D16), D16207, doi:10.1029/2006JD007076, 2006.

1064 Schwarz, J. P., Spackman, J. R., Gao, R. S., Perring, A. E., Cross, E., Onasch, T. B., Ahern, A.,
1065 Wrobel, W., Davidovits, P., Olfert, J., Dubey, M. K., Mazzoleni, C. and Fahey, D. W.: The
1066 Detection Efficiency of the Single Particle Soot Photometer, Aerosol Sci. Technol., 44(8), 612–
1067 628, doi:10.1080/02786826.2010.481298, 2010.

1068 Sedlacek III, A. J., Buseck, P. R., Adachi, K., Onasch, T. B., Springston, S. R. and Kleinman, L.:
1069 Formation and evolution of tar balls from northwestern US wildfires, Atmos. Chem. Phys.,
1070 18(15), 11289–11301, doi:10.5194/acp-18-11289-2018, 2018.

1071 Selimovic, V., Yokelson, R. J., Warneke, C., Roberts, J. M., de Gouw, J., Reardon, J. and
1072 Griffith, D. W. T.: Aerosol optical properties and trace gas emissions by PAX and OP-FTIR for
1073 laboratory-simulated western US wildfires during FIREX, Atmos. Chem. Phys., 18(4), 2929–
1074 2948, doi:10.5194/acp-18-2929-2018, 2018.

1075 Sharma, S., Richard Leaitch, W., Huang, L., Veber, D., Kolonjari, F., Zhang, W., Hanna, S. J.,
1076 Bertram, A. K. and Ogren, J. A.: An evaluation of three methods for measuring black carbon in
1077 Alert, Canada, Atmos. Chem. Phys., 17(24), 15225–15243, doi:10.5194/acp-17-15225-2017,
1078 2017.

1079 Sheridan, P. J., Arnott, W. P., Ogren, J. A., Andrews, E., Atkinson, D. B., Covert, D. S.,
1080 Moosmüller, H., Petzold, A., Schmid, B., Strawa, A. W., Varma, R. and Virkkula, A.: The Reno
1081 Aerosol Optics Study: An Evaluation of Aerosol Absorption Measurement Methods, Aerosol Sci.
1082 Technol., 39(1), 1–16, doi:10.1080/027868290901891, 2005.

1083 Slowik, J. G., Cross, E. S., Han, J.-H., Davidovits, P., Onasch, T. B., Jayne, J. T., Williams, L. R.,
1084 Canagaratna, M. R., Worsnop, D. R., Chakrabarty, R. K., Moosmüller, H., Arnott, W. P.,
1085 Schwarz, J. P., Gao, R.-S., Fahey, D. W., Kok, G. L. and Petzold, A.: An Inter-Comparison of

Instruments Measuring Black Carbon Content of Soot Particles, Aerosol Sci. Technol., 41(3), 295–314, doi:10.1080/02786820701197078, 2007.

Solomon, P. A., Crumpler, D., Flanagan, J. B., Jayanty, R. K. M., Rickman, E. E. and McDade, C. E.: U.S. National PM 2.5 Chemical Speciation Monitoring Networks—CSN and IMPROVE: Description of networks, J. Air Waste Manage. Assoc., 64(12), 1410–1438, doi:10.1080/10962247.2014.956904, 2014.

Spackman, J. R., Schwarz, J. P., Gao, R. S., Watts, L. A., Thomson, D. S., Fahey, D. W., Holloway, J. S., de Gouw, J. A., Trainer, M. and Ryerson, T. B.: Empirical correlations between black carbon aerosol and carbon monoxide in the lower and middle troposphere, Geophys. Res. Lett., 35(19), L19816, doi:10.1029/2008GL035237, 2008.

Spinazzè, A., Fanti, G., Borghi, F., Del Buono, L., Campagnolo, D., Rovelli, S., Cattaneo, A. and Cavallo, D. M.: Field comparison of instruments for exposure assessment of airborne ultrafine particles and particulate matter, Atmos. Environ., 154, 274–284, doi:10.1016/j.atmosenv.2017.01.054, 2017.

Subramanian, R., Roden, C. A., Boparai, P. and Bond, T. C.: Aerosol Science and Technology Yellow Beads and Missing Particles: Trouble Ahead for Filter-Based Absorption Measurements Yellow Beads and Missing Particles: Trouble Ahead for Filter-Based Absorption Measurements, Aerosol Sci. Technol., 41, 630–637, doi:10.1080/02786820701344589, 2007.

Virkkula, A.: Correction of the Calibration of the 3-wavelength Particle Soot Absorption Photometer (3λ PSAP), Aerosol Sci. Technol., 44(8), 706–712, doi:10.1080/02786826.2010.482110, 2010.

Virkkula, A., Ahlquist, N. C., Covert, D. S., Arnott, W. P., Sheridan, P. J., Quinn, P. K. and Coffman, D. J.: Modification, calibration and a field test of an instrument for measuring light absorption by particles, Aerosol Sci. Technol., 39(1), 68–83, doi:10.1080/027868290901963, 2005.

Wang, R., Balkanski, Y., Boucher, O., Ciais, P., Schuster, G. L., Chevallier, F., Samset, B. H., Liu, J., Piao, S., Valari, M. and Tao, S.: Estimation of global black carbon direct radiative forcing and its uncertainty constrained by observations, J. Geophys. Res. Atmos., 121(10), 5948–5971, doi:10.1002/2015JD024326, 2016.

Ward, T. J., Hamilton, R. F., Dixon, R. W., Paulsen, M. and Simpson, C. D.: Characterization and evaluation of smoke tracers in PM: Results from the 2003 Montana wildfire season, Atmos. Environ., 40(36), 7005–7017, doi:10.1016/j.atmosenv.2006.06.034, 2006.

Watson, J. G., Chow, J. C. and Chen, L. A.: Summary of Organic and Elemental Carbon / Black

Carbon Analysis Methods and Intercomparisons., 2005.

Weingartner, E., Saathoff, H., Schnaiter, M., Streit, N., Bitnar, B. and Baltensperger, U.: Absorption of light by soot particles: Determination of the absorption coefficient by means of aethalometers, J. Aerosol Sci., 34(10), 1445–1463, doi:10.1016/S0021-8502(03)00359-8, 2003.

Wu, C. and Yu, J. Z.: Evaluation of linear regression techniques for atmospheric applications: the importance of appropriate weighting, Atmos. Meas. Tech., 11(2), 1233–1250, doi:10.5194/amt-11-1233-2018, 2018.

Yelverton, T. L. B., Hays, M. D., Gullett, B. K. and Linak, W. P.: Black Carbon Measurements of Flame-Generated Soot as Determined by Optical, Thermal-Optical, Direct Absorption, and Laser Incandescence Methods, Environ. Eng. Sci., 31(4), 209–215, doi:10.1089/ees.2014.0038, 2014.

Yeung, K. Y., Haynor, D. R. and Ruzzo, W. L.: Validating clustering for gene expression data, Bioinformatics, 17(4), 309–318, doi:10.1093/bioinformatics/17.4.309, 2001.

Yokelson, R. J., Griffith, D. W. T. and Ward, D. E.: Open-path Fourier transform infrared studies of large-scale laboratory biomass fires, J. Geophys. Res. Atmos., 101(D15), 21067–21080, doi:10.1029/96JD01800, 1996.

Yokelson, R. J., Crounse, J. D., DeCarlo, P. F., Karl, T., Urbanski, S., Atlas, E., Campos, T., Shinozuka, Y., Kapustin, V., Clarke, A. D., Weinheimer, A., Knapp, D. J., Montzka, D. D., Holloway, J., Weibring, P., Flocke, F., Zheng, W., Toohey, D., Wennberg, P. O., Wiedinmyer, C., Mauldin, L., Fried, A., Richter, D., Walega, J., Jimenez, J. L., Adachi, K., Buseck, P. R., Hall, S. R. and Shetter, R.: Emissions from biomass burning in the Yucatan, Atmos. Chem. Phys., 9(15), 5785–5812, doi:10.5194/acp-9-5785-2009, 2009.